J. Fluid Mech. (2002), *vol.* 467, *pp.* 129–161. © 2002 Cambridge University Press
DOI: 10.1017/S0022112002001301 Printed in the United Kingdom

Adjoint-based optimization of steady suction for disturbance control in incompressible flows

By JAN O. PRALITS[1,2], A. HANIFI[2] AND D. S. HENNINGSON[1,2]

[1]Department of Mechanics, KTH, SE-100 44 Stockholm, Sweden

[2]Swedish Defence Research Agency, FOI, Aeronautics Division, FFA, SE-172 90 Stockholm, Sweden

(Received 7 May 2001 and in revised form 25 March 2002)

The optimal distribution of steady suction needed to control the growth of single or multiple disturbances in quasi-three-dimensional incompressible boundary layers on a flat plate is investigated. The evolution of disturbances is analysed in the framework of the parabolized stability equations (PSE). A gradient-based optimization procedure is used and the gradients are evaluated using the adjoint of the parabolized stability equations (APSE) and the adjoint of the boundary layer equations (ABLE). The accuracy of the gradient is increased by introducing a stabilization procedure for the PSE. Results show that a suction peak appears in the upstream part of the suction region for optimal control of Tollmien–Schlichting (T–S) waves, steady streamwise streaks in a two-dimensional boundary layer and oblique waves in a quasi-three-dimensional boundary layer subject to an adverse pressure gradient. The mean flow modifications due to suction are shown to have a stabilizing effect similar to that of a favourable pressure gradient. It is also shown that the optimal suction distribution for the disturbance of interest reduces the growth rate of other perturbations. Results for control of a steady cross-flow mode in a three-dimensional boundary layer subject to a favourable pressure gradient show that not even large amounts of suction can completely stabilize the disturbance.

1. Introduction

Laminar–turbulent transition in boundary layers on aircraft causes a rapid increase of the skin friction and consequently a larger drag. Therefore, delay of transition occurrence will reduce the fuel consumption which results in a lower operation cost and less pollution. Transition in the boundary layer on aircraft wings is usually caused by breakdown of small disturbances which grow as they propagate downstream. It is well known that the growth of such disturbances can be suppressed or controlled by steady or unsteady wall suction. The latter is sometimes referred to as the wave-cancellation concept and has been investigated both numerically and experimentally by numerous authors, see Joslin (1998) for an excellent overview of earlier experimental and numerical works.

Steady suction implies a modification of the steady mean flow. Here, the aim is to reduce the thickness of the boundary layer and to stabilize the mean velocity profile. The inviscid instability in two-dimensional boundary layers, which is related to the second wall-normal derivative of the streamwise velocity, is stabilized by suction. A similar stabilizing effect is obtained by imposing a favourable pressure gradient

https://doi.org/10.1017/S0022112002001301 Published online by Cambridge University Press

given zero suction on the wall. The relation between suction, the pressure gradient and the viscous terms in two-dimensional boundary layers is explained well in e.g. Schlichting (1979). The mean flow obtained using non-zero suction has similarities with that obtained when a negative pressure gradient is applied. In the case of an adverse pressure gradient present in the flow, the superposition of suction will reduce the curvature of the velocity profile at the wall, weakening the inflection in the profile which inhibits the inviscid instability. It should be noted that the discussion above relates primarily to exponential instabilities.

Constant steady suction has been studied both experimentally and numerically by several authors. Iglisch (1949) investigated theoretically the initial length needed for the shape factor (displacement thickness/momentum thickness) to reach a constant value in the case of a flat-plate two-dimensional boundary layer. Here, the streamwise velocity profile becomes 'fuller' downstream as suction is applied, finally reaching the so-called 'asymptotic suction profile'. With the assumption of an asymptotic velocity profile along the whole plate, the laminar boundary layer is stable with respect to two-dimensional T–S wave instabilities if the constant suction velocity $V_w = V_w^\star/U_\infty^\star = 1.4 \times 10^{-5}$. Here, $V_w^\star$ and $U_\infty^\star$ are the dimensional wall-normal suction velocity at the wall and free-stream velocity components of the mean flow, respectively. For the same case, Ulrich (1944) showed that the critical Reynolds number, Re_{crit}, decreases as the leading edge is approached. Hence, an increasing amount of suction is required in this region. In Schlichting (1979) it was shown that a correction due to increased suction close to the leading edge leads to a constant suction velocity $V_w = 1.2 \times 10^{-4}$ in order to maintain a laminar flow along the whole plate. The increased suction velocity due to the correction of the initial length means an increased amount of suction energy. If a large amount of suction is applied then the power saved by the reduction in drag might well be lost by the power used for the suction device. Further, if a large amount of suction is used, resulting in a thinning of the boundary layer, then this may lead to an increase of the shear stress at the wall. It is therefore of interest to investigate if a more optimal suction distribution can be obtained which meets the objective of reducing the disturbances present in the flow while using the least amount of suction energy.

In the past decade more interest has been focused on optimal control of fluid flows in which optimal control theory has been utilized in different manners. Here, the objective is to minimize some measure of the state with a prescribed amount of suction on the wall. This can mathematically be described by a minimization of an objective function which balances a measure of the state and a measure of the control. The problem can be solved using the sensitivity information given by the gradient of the objective function with respect to the control in a gradient-based optimization routine. An efficient way to calculate the gradients is the adjoint approach which has proved successful in numerous applications such as shape optimization, optimal control, receptivity, meteorology and optimal perturbations as long as the number of constraints are low and the control-variable space is large. A recent workshop on adjoint systems, see *Flow, Turbulence and Combustion*, Vol. 65 (3/4), 2000, indicates some of the progress in the field.

Here the wall-normal velocity component of the steady mean flow on the wall is used as the control, which means that the suction will modify the mean flow to control disturbance growth rather than generating an out-of phase disturbance by time-periodic suction. Balakumar & Hall (1999) used a Lagrangian approach to find the optimal suction distribution for Blasius and swept Hiemenz flows. The objective was to move the transition point, given by the e^N-method, downstream. They found

https://doi.org/10.1017/S0022112002001301 Published online by Cambridge University Press

that for Blasius boundary layers the optimal suction distribution peaked upstream of the maximum growth rate and decreased to zero at the transition point.

In the present work we use an approach different from that in Balakumar & Hall (1999). The control problem is defined using optimal control theory in which a gradient-based technique is used to update the control during the optimization process. The aim is to minimize a given objective function balancing a measure of the total disturbance kinetic energy and the control energy. The mean flow is found by solving the quasi-three-dimensional boundary layer equations for incompressible flows and the growth of disturbances is analysed for developing boundary layers using the parabolized stability equations (PSE) (see Bertolotti, Herbert & Spalart 1992; Malik & Balakumar 1992; Simen 1992; Herbert 1997). In the framework of these governing equations we can analyse convective instabilities under the assumption of a slow variation of both the mean flow and the shape function of the disturbances in the streamwise direction. We also assume that the streamwise pressure distribution is not affected by suction at the wall. The mean flow is obtained using the boundary layer equations (see e.g. Schlichting 1979). In this approximation, as well as in higher-order approximations, the wall-normal velocity of the mean flow, V, is $O(1/Re)$. Here $Re = U_\infty^\star l^\star / v^\star$ is the Reynolds number in which $l^\star$ and $v^\star$ denote the dimensional reference length and kinematic viscosity, respectively. In the optimization one must make sure that this assumption is not violated.

An adjoint-based technique is used to evaluate the gradients (sensitivities). Here, we couple the adjoint of the PSE with the adjoint of the boundary layer equations in order to find the gradient of the disturbance growth due to modifications of the mean flow. The use of the adjoint PSE (APSE) was first proposed by Herbert (1997) and has since been used for receptivity studies (see Hill 1997*a*; Airiau 2000; Dobrinsky & Collis 2000), sensitivity analysis (see Pralits *et al.* 2000*a*) and optimal control problems (see Hill 1997*b*; Pralits, Hanifi & Henningson 2000*b*; Walther, Airiau & Bottaro 2001). Hill (1997*b*) used a similar approach in inverse design for laminar boundary layers. However, no details were given there. The common interest of all these applications lies in the efficient evaluation of receptivity coefficients and sensitivity information provided by a single solution of the APSE. The major difference between previous works is in the derivation of the APSE. In Hill (1997*a*, *b*), Airiau (2000) and Dobrinsky & Collis (2000) the APSE is an approximation of the adjoint of the linearized Navier–Stokes equations given an ansatz similar to the PSE. The additional equation used to find the 'adjoint' streamwise wavenumber comes from an orthogonality relation between the solutions from the APSE and PSE. In Dobrinsky & Collis (2000) it is shown that this condition in fact does not hold in a large part of the domain which means a less accurate adjoint equation. This is said to depend on the numerical scheme and approximate inflow conditions. In Pralits *et al.* (2000*a*) the APSE is derived directly from the PSE using a variational technique and the additional equation and inflow conditions are part of the definition of the adjoint operator. The latter technique, which is shown to have good accuracy in the major part of the domain, is also used in Pralits *et al.* (2000*b*) and Walther *et al.* (2001).

The optimization process is dependent on the accuracy of the gradient (search direction), which can be evaluated to better assess the optimization results. In the present work, the gradient is derived from the continuous state equations which means that its accuracy can be improved if the resolution is increased, see e.g. Högberg & Berggren (2000). However, the PSE is known to be unstable for small streamwise steps due to the remaining ellipticity. Several studies on how to stabilize the PSE have been done (see Haj-Hariri 1994; Li & Malik 1994, 1996; Andersson, Henningson &

https://doi.org/10.1017/S0022112002001301 Published online by Cambridge University Press

Hanifi 1998). The approach which best removes the ellipticity while still producing an accurate result is the technique introduced by Andersson *et al.* (1998), where originally neglected higher-order terms, $O(Re^{-2})$, are reintroduced. This stabilization procedure will also affect the adjoint equations (see § 2.4).

In this paper we present a method which involves solving a number of problems regarding the derivation of the gradient, adjoint equations and stabilization of the adjoint equations. For this reason, a large part of the paper is dedicated to explaining the different steps in detail. The optimal control problem and the corresponding equations are presented in § 2. In § 3, the adjoint equations are validated by analysing the gradient accuracy. Here we also show results on optimal control of steady streamwise streaks and T–S waves in a two-dimensional boundary layer, and oblique waves and a steady cross-flow mode in a quasi-three-dimensional boundary layer. The discussion and concluding remarks are given in § 4 and the complete derivation of the gradient and the coupling of the adjoint of the parabolized stability and boundary layer equations are shown in Appendix B. A preliminary version of the work presented here can be found in the report by Pralits *et al.* (2000*b*).

2. Problem formulation

This section presents the optimal control problem for incompressible flows. For simplicity, we restrict our analysis to a plane geometry.

2.1. *State equations*

The flow field is given by the solution of the mass and momentum conservation equations for a viscous flow. The equations are written for a Cartesian coordinate system with streamwise, normal and spanwise coordinates denoted as x, y and z, respectively. The flow field is decomposed into a mean, Q, and a perturbation part, q, as

$$Q_{tot}(x, y, z, t) = Q(x, y) + q(x, y, z, t),$$

where $Q = (U, V, W, P)^T$ and $q = (u, v, w, p)^T$. The mean flow, which has zero variation in the spanwise direction, is a three-component, two-dimensional boundary layer and is here referred to as a quasi-three-dimensional boundary layer. The evolution of disturbances is analysed in the framework of the non-local stability theory (see e.g. Bertolotti *et al.* 1992; Malik & Balakumar 1992; Simen 1992; Herbert 1997).

In the following sections the equations for the mean flow and disturbances, in non-dimensional form, are given. The velocity components are made non-dimensional by $U^\star_\infty$, the pressure by $\rho^\star U^{\star 2}_\infty$ and the reference length is taken as $l^\star_0 = (\nu^\star x^\star_0 / U^\star_\infty)^{1/2}$. Here superscript * denotes dimensional quantities, $\nu^\star$ the kinematic viscosity, $U^\star_\infty$ the free-stream velocity and $\rho^\star$ the density.

2.1.1. *Mean flow equations*

The non-dimensional boundary layer equations for a quasi-three-dimensional incompressible flow on a flat plate with an external pressure gradient given as $\mathrm{d}P_e/\mathrm{d}x = -U_e \mathrm{d}U_e/\mathrm{d}x$ can be written

$$\frac{\partial U}{\partial x} + \frac{\partial V}{\partial y} = 0, \tag{2.1}$$

https://doi.org/10.1017/S0022112002001301 Published online by Cambridge University Press

$$U\frac{\partial U}{\partial x}+V\frac{\partial U}{\partial y}-U_e\frac{\mathrm{d}U_e}{\mathrm{d}x}-\frac{1}{Re}\frac{\partial^2 U}{\partial y^2}=0, \tag{2.2}$$

$$U\frac{\partial W}{\partial x}+V\frac{\partial W}{\partial y}-\frac{1}{Re}\frac{\partial^2 W}{\partial y^2}=0, \tag{2.3}$$

with the boundary conditions

$$\left.\begin{array}{rl} U=W=0,\ V=V_{\mathrm{w}} & \text{on}\quad y=0,\\ (U,W)\to(U_e,W_e) & \text{as}\quad y\to\infty, \end{array}\right\} \tag{2.4}$$

where index e denotes that the variable is evaluated at the boundary layer edge and $Re=l_0^\star U_\infty^\star/\nu^\star$ is the Reynolds number. Note that for the boundary layer approximations to be valid, the normal velocity at the wall, $V_{\mathrm{w}}=V_{\mathrm{w}}^\star/U_\infty^\star$, should be $O(Re^{-1})$.

2.1.2. *Disturbance equations*

We assume the perturbations to be time and spanwise periodic disturbances:

$$q(x,y,z,t)=\hat{q}(x,y)\exp\mathrm{i}\left(\int_{X_0}^{x'}\alpha\,\mathrm{d}x'+\beta z-\omega t\right)+\text{c.c.}, \tag{2.5}$$

where α is the complex streamwise wavenumber, β the real spanwise wavenumber and ω the real disturbance angular frequency. We assume a scale separation Re^{-1} between the weak variation in the x-direction and the strong variation in the y-direction. It is also assumed that $\partial/\partial x\sim O(Re^{-1})$ and $V\sim O(Re^{-1})$. Introducing (2.5) and the assumptions above in the linearized governing equations and keeping terms up to $O(Re^{-1})$, yields a set of nearly parabolic partial differential equations

$$\boldsymbol{A}\hat{q}+\boldsymbol{B}\frac{\partial\hat{q}}{\partial y}+\boldsymbol{C}\frac{\partial^2\hat{q}}{\partial y^2}+\boldsymbol{D}\frac{\partial\hat{q}}{\partial x}=0, \tag{2.6}$$

where the matrices $\boldsymbol{A},\boldsymbol{B},\boldsymbol{C}$ and $\boldsymbol{D}$ are given in Appendix A. For a note on the parabolic nature of the PSE see Bertolotti *et al.* (1992), Haj-Hariri (1994), Li & Malik (1994, 1996) and Andersson *et al.* (1998). To remove the ambiguity of having x-dependence of both the amplitude function and wave function in (2.5) and to maintain a slow variation of the amplitude function $\hat{q}$, a so-called 'auxiliary condition' is introduced:

$$\int_0^\infty \hat{\boldsymbol{u}}^H\frac{\partial\hat{\boldsymbol{u}}}{\partial x}\,\mathrm{d}y=0, \tag{2.7}$$

where $\hat{\boldsymbol{u}}=(\hat{u},\hat{v},\hat{w})^T$ and superscript H denotes the complex conjugate transpose. The disturbances are subjected to the following boundary conditions:

$$\left.\begin{array}{ll} \hat{\boldsymbol{u}}=0 & \text{on}\quad y=0\\ \hat{\boldsymbol{u}}\to 0 & \text{as}\quad y\to\infty. \end{array}\right\} \tag{2.8}$$

The system of equations (2.6) and (2.7) is integrated in the downstream direction with the initial condition given by the solution of the local stability theory at $x=X_0$. At each streamwise position, the value of α is iterated such that (2.7) is satisfied.

2.2. *Optimal control of a single disturbance*

In this section, we define an optimal control problem where the mean normal velocity at the wall is optimized to reduce the growth of a single disturbance with a fixed given

https://doi.org/10.1017/S0022112002001301 Published online by Cambridge University Press

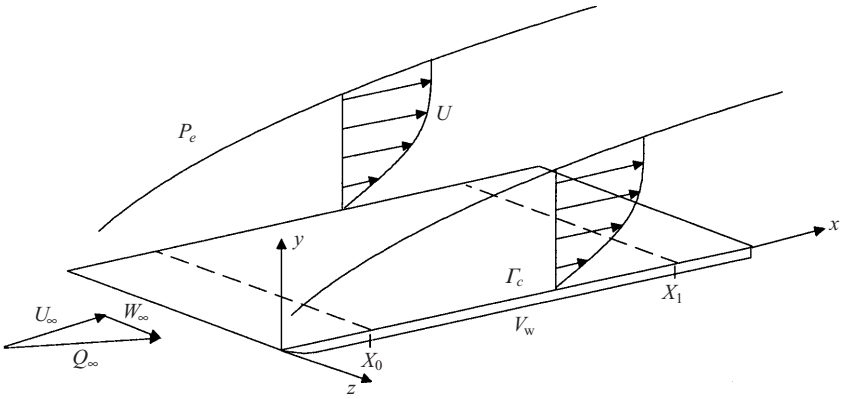


FIGURE 1. Computational domain: flat-plate boundary layer.

initital condition. The optimization problem is solved by minimizing an objective function balancing a measure of the state and the control using a gradient-based method. We obtain the gradient of the objective function using an adjoint technique. The complete derivation of the equations can be found in Appendix B.

2.2.1. *Objective function*

We measure the size of a disturbance in domain Ω, defined such that $x \in [X_0, X_1]$, $y \in [0, \infty)$ and $z \in [Z_0, Z_1]$ (see figure 1), by its total kinetic energy defined as

$$E = \frac{1}{2}\int_{Z_0}^{Z_1}\int_{X_0}^{X_1}\int_0^{\infty} \boldsymbol{u}^T\boldsymbol{u}\,\mathrm{d}y\,\mathrm{d}x\,\mathrm{d}z.$$

The objective function to be minimized is

$$J(V_w) = \frac{1}{2}\int_{Z_0}^{Z_1}\int_{X_0}^{X_1}\int_0^{\infty} \boldsymbol{u}^T\boldsymbol{u}\,\mathrm{d}y\,\mathrm{d}x\,\mathrm{d}z + \frac{l^2}{2}\int_{Z_0}^{Z_1}\int_{X_0}^{X_1} {V_w}^2\,\mathrm{d}x\,\mathrm{d}z, \tag{2.9}$$

where $l^2 > 0$ is the regularization parameter and is used to ensure that the size of the control parameter V_w does not grow unbounded. Now, the control problem can be defined mathematically as

$$\text{find} \quad V_w^{opt} \in L^2(\Gamma_c) \quad \text{such that}$$
$$J(V_w^{opt}) \leqslant J(V_w)\,\forall\, V_w \in L^2(\Gamma_c), \tag{2.10}$$

where V_w^{opt} is the optimal suction distribution on the wall.

2.2.2. *Adjoint equations and the gradient*

The gradient of the objective function (2.9) with respect to the control variable is defined through the directional derivative as

$$\delta J = \langle \nabla_{V_w} J, \delta V_w \rangle = \lim_{s\to 0}\left|\frac{J(V_w + s\delta V_w) - J(V_w)}{s}\right|, \tag{2.11}$$

where δV_w is the variation of the control variable. Here, we derive the gradient expression using the adjoint of the state equations. Details of the derivation are given in Appendix B. This yields

$$\nabla_{V_w} J = l^2 V_w + V_w^* \quad \text{on} \quad y = 0. \tag{2.12}$$

https://doi.org/10.1017/S0022112002001301 Published online by Cambridge University Press

The value of $V_{\mathrm{w}}^{*} = V^{*}(x,0)$ in (2.12) is given by the solution of the adjoint of the PSE and boundary layer equations, hereafter referred to as APSE and ABLE, respectively. The APSE which is given by (B 11)–(B 15) in Appendix B is here written

$$\boldsymbol{A}^{H} q^{*} - \boldsymbol{B}^{H} \frac{\partial q^{*}}{\partial y} + \boldsymbol{C}^{H} \frac{\partial^{2} q^{*}}{\partial y^{2}} - \boldsymbol{D}^{H} \frac{\partial q^{*}}{\partial x} = f_{APSE}, \tag{2.13}$$

$$\frac{\partial}{\partial x} \int_{0}^{\infty} q^{*H} \frac{\partial \boldsymbol{A}}{\partial \alpha} \hat{q} \, \mathrm{d}y + \mathrm{i}|\Theta|^{2} \int_{0}^{\infty} |\hat{\boldsymbol{u}}|^{2} \, \mathrm{d}y = 0, \tag{2.14}$$

with boundary conditions

$$\left.\begin{aligned} u^{*} = v^{*} = w^{*} = 0 \quad \text{on} \quad y = 0, \\ u^{*}, v^{*}, w^{*} \to 0 \quad \text{as} \quad y \to \infty, \end{aligned}\right\} \tag{2.15}$$

and initial conditions

$$q^{*} = r^{*} = 0 \quad \text{on} \quad x = X_{1}. \tag{2.16}$$

Here, $q^{*} = (p^{*}, u^{*}, v^{*}, w^{*})^{T}$ and r^{*} are the co-state variables and f_{APSE} is the forcing due to the auxiliary condition of the PSE and the objective function. Equations (2.13)–(2.14) are integrated in the upstream direction starting at $x = X_{1}$. At each streamwise position, the value of the scalar r^{*} is iteratively found such that (2.14) is satisfied. The ABLE, given by (B 16)–(B 18), are satisfied by the co-state variables $Q^{*} = (U^{*}, V^{*}, W^{*})$. They are here written as

$$L_{BLE}^{*}(Q) Q^{*} = f_{ABLE}, \tag{2.17}$$

with boundary conditions

$$\left.\begin{aligned} U^{*} = W^{*} = 0 \quad \text{on} \quad y = 0, \\ U^{*}, V^{*}, W^{*} \to 0 \quad \text{as} \quad y \to \infty, \end{aligned}\right\} \tag{2.18}$$

and initial conditions

$$U^{*} = V^{*} = W^{*} = 0 \quad \text{on} \quad x = X_{1}. \tag{2.19}$$

The forcing term in (2.17), f_{ABLE}, is a function of the solutions of both the PSE and the APSE. Equation (2.17) is integrated in the upstream direction starting at $x = X_{1}$. The optimization procedure can now be outlined as the following steps, see the chart given in figure 2, where k denotes the iteration number.

(i) The BLE (2.1)–(2.3) are integrated from $x = X_{0}$ to $x = X_{1}$. If $k = 1$ then $V_{\mathrm{w}}^{k} = 0$ (initial guess for the suction distribution).

(ii) The PSE (2.6)–(2.7) are integrated from $x = X_{0}$ to $x = X_{1}$, then the APSE are integrated from $x = X_{1}$ to $x = X_{0}$.

(iii) f_{ABLE} is calculated from the solution of both the PSE and APSE.

(iv) The ABLE (2.17) is integrated from $x = X_{1}$ to $x = X_{0}$ given the forcing, f_{ABLE}, from (iii).

(v) If $k < 2$ then goto (vi), else evaluate the convergence criteria: If $J^{k+1} - J^{k} < err$ then convergence is reached else goto (vi). Here *err* is a small real-valued parameter defining the convergence.

(vi) The gradient, (2.12), is evaluated and the new boundary condition for the BLE, V_{w}^{k+1}, is calculated using an optimization routine (here we use a limited-memory quasi-Newton method). Continue: $k = k + 1$, goto (i).

https://doi.org/10.1017/S0022112002001301 Published online by Cambridge University Press

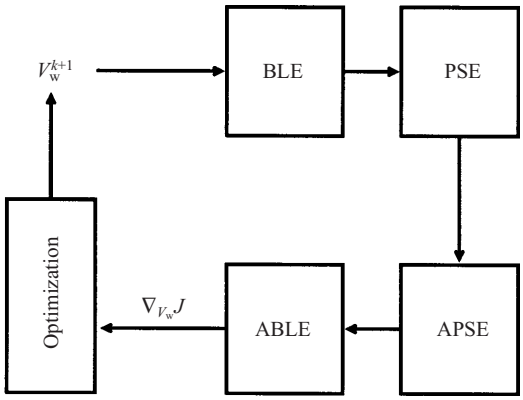


FIGURE 2. Chart of the solution process.

The gradient of the objective function due to a variation of the free-stream velocity can be derived in the same manner as for V_w and yields

$$\nabla_{U_e} J = -U_e \int_0^\infty \frac{\partial U^*}{\partial x} \, \mathrm{d}y. \tag{2.20}$$

This variation would be the result of a change in the geometry and consequently the pressure distribution. Effects due to geometry changes are not investigated here.

2.3. *Optimal control of multiple disturbances*

In this section we generalize the technique introduced above to find the optimal suction distribution of the steady mean flow that accounts for the growth of more than one disturbance. This is necessary for cases where it is not possible to clearly state which disturbance will grow the most and thus cause laminar–turbulent transition first. An example of this is the two-dimensional Blasius boundary layer where either T–S wave-type instabilities or steady streamwise streaks could give the maximum growth at a given streamwise position. The measure of disturbance kinetic energy in Ω is now taken as the sum of the energy of a chosen number of pre-defined disturbances in a convectively unstable flow. In this case, the suction distribution will be optimal for the sum of these disturbances. Our approach is however different from non-cooperative strategies (see Bewley & Liu 1998; Bewley & Moin 1997) which analyse worst-case scenarios, so-called robust control. There, the strategy is to find the best control in the presence of the worst-case external disturbance.

The analysis here does not differ much from the one outlined in § 2.2 and is therefore done in a more compact form here. If we denote the total number of existing disturbances by N then the total kinetic energy is defined as

$$E = \sum_{k=1}^{N} \frac{1}{2} \int_{Z_0}^{Z_1} \int_{X_0}^{X_1} \int_0^\infty \boldsymbol{u}_k^T \boldsymbol{u}_k \, \mathrm{d}y \, \mathrm{d}x \, \mathrm{d}z.$$

The objective function to be minimized is now

$$J(V_w) = \sum_{k=1}^{N} \frac{1}{2} \int_{Z_0}^{Z_1} \int_{X_0}^{X_1} \int_0^\infty \boldsymbol{u}_k^T \boldsymbol{u}_k \, \mathrm{d}y \, \mathrm{d}x \, \mathrm{d}z + \frac{l^2}{2} \int_{Z_0}^{Z_1} \int_{X_0}^{X_1} {V_w}^2 \, \mathrm{d}x \, \mathrm{d}z. \tag{2.21}$$

The same procedure to find the gradient of J with respect to V_w as given in Appendix B

https://doi.org/10.1017/S0022112002001301 Published online by Cambridge University Press

for control of single disturbances is now used to account for several disturbances. As the control problem is derived for steady suction, the case of multiple disturbances does not introduce any further complications. Equation (2.11) is used to define the gradient which can now be written

$$\nabla_{V_w} J = l^2 V_w + \sum_{k=1}^{N} (V_w^*)_k \quad \text{on} \quad y = 0. \tag{2.22}$$

Equation (2.22) implies that each equation in the solution procedure given in figure 2 must be solved N times, i.e. for each disturbance, before evaluating the gradient. Instead, one can use the fact that the ABLE are linear equations. In this case, for a given solution of the BLE, the PSE and the APSE are solved N times, step (ii) related to figure 2. The forcing term of the ABLE, step (iii), is then computed as the sum of N realizations. In step (iv), the ABLE are solved once given the total forcing from all N disturbances. The gradient is finally evaluated from (2.12) which was given for control of single disturbances. However, now a single evaluation of V_w^* accounts for all N disturbances.

It should be mentioned that the evaluation of the initial disturbances far upstream of the neutral point may be difficult. Therefore, if we consider a large number of different disturbances whose neutral points are widely spread in the streamwise direction, care has to be taken when X_0 is chosen.

2.4. *Adjoint of the stabilized PSE*

In gradient-based optimization, an increased accuracy of the gradient will give a result closer to the optimum. The gradient presented here, (2.12), is derived using a so-called continuous approach. This means that the adjoint of a state equation is derived from the continuous equation and then discretized. Another approach is to first discretize the state equation and then derive its adjoint, the so-called discrete approach. The latter yields a more accurate gradient in most cases but its derivation is more complicated. However, results of the continuous approach should converge to those of the discrete one as the grid resolution is refined (see Högberg & Berggren 2000). It is well-known that the PSE become unstable as the grid in the streamwise direction is refined due to ellipticity remaining in the equations (see Haj-Hariri 1994; Li & Malik 1994, 1996; Andersson *et al.* 1998). This problem will therefore put a limit on the accuracy of the gradient unless some technique is used to overcome the instability problem and allow a smaller step size in the streamwise direction. A stabilization procedure was presented by Andersson *et al.* (1998) in which they add terms proportional to the truncation error of the implicit scheme used in the streamwise direction. These terms are of the same order as some of the originally neglected terms in the PSE. It was shown that the procedure does not alter the PSE results while allowing higher streamwise resolution. The procedure here, however, not only adds terms to the PSE but also affects all adjoint equations since we derive the adjoint from the PSE and not the adjoint linearized Navier–Stokes equations. Here, we present an outline of how to derive the PSE, gradient and adjoint equations, using the stabilization technique given by Andersson *et al.* The details of the derivation can be seen in Appendix B, § B.3. Following Andersson *et al.*, terms $O(Re^{-2})$ are introduced in (2.6). The stabilized PSE can be written

$$-\boldsymbol{D}\frac{\partial \hat{q}}{\partial x} = \boldsymbol{A}\left[\hat{q} + s\frac{\partial \hat{q}}{\partial x}\right] + \boldsymbol{B}\left[\frac{\partial \hat{q}}{\partial y} + s\frac{\partial}{\partial x}\left(\frac{\partial \hat{q}}{\partial y}\right)\right] + \boldsymbol{C}\left[\frac{\partial^2 \hat{q}}{\partial y^2} + s\frac{\partial}{\partial x}\left(\frac{\partial^2 \hat{q}}{\partial y^2}\right)\right], \tag{2.23}$$

https://doi.org/10.1017/S0022112002001301 Published online by Cambridge University Press

where s is a positive real number. The gradient (2.12) and the adjoint equations were derived in Appendix B without the stabilization terms. Now, the derivation has to be performed using (2.23) instead of (2.6) which yields the following adjoint equations:

$$-\boldsymbol{D}^H\frac{\partial q^*}{\partial x} = -\left[\boldsymbol{A}^H q^* - s\tilde{\boldsymbol{A}}^H\frac{\partial q^*}{\partial x}\right] + \boldsymbol{B}^H\left[\frac{\partial q^*}{\partial y} - s\frac{\partial}{\partial x}\left(\frac{\partial q^*}{\partial y}\right)\right] - \boldsymbol{C}^H\left[\frac{\partial^2 q^*}{\partial y^2} - s\frac{\partial}{\partial x}\left(\frac{\partial^2 q^*}{\partial y^2}\right)\right] + f_{APSE}, \quad (2.24)$$

$$\frac{\partial}{\partial x}\int_0^\infty q^{*H}\frac{\partial \boldsymbol{A}}{\partial \alpha}\left[\hat{q} + s\frac{\partial \hat{q}}{\partial x}\right]\mathrm{d}y + \mathrm{i}|\Theta|^2\int_0^\infty |\hat{\boldsymbol{u}}|^2\,\mathrm{d}y = 0, \quad (2.25)$$

$$L^*_{BLE}(Q)Q^* = \tilde{f}_{ABLE}, \quad (2.26)$$

where f_{APSE} and f_{ABLE} denotes the forcing terms of the APSE and ABLE respectively and the tilde marks where additional terms due to the stabilization procedure appear. Note here that there is no influence on the gradient expression or on the boundary conditions of the state and adjoint equations due to the stabilizing terms. The additional terms on the right-hand side of (2.24) resemble the stabilizing terms in (2.23) apart from the sign difference on s. The APSE resembles the PSE and the new right-hand side of (2.24) will indeed be a stabilizing term allowing a smaller step size in the streamwise direction and the calculation of a more accurate gradient.

3. Results

The results presented are obtained by numerically integrating the discretized state and co-state (adjoint) equations. The x-derivatives are approximated by a first- or second-order-accurate backward Euler scheme. The y-derivatives of the PSE and APSE are approximated by Chebychev-polynomials and a second-order-accurate finite-difference scheme for the BLE and ABLE. The L-BFGS-B package, which is based on the limited memory quasi-Newton method, is used in the optimization procedure (see Zhu *et al.* 1994; Byrd *et al.* 1995). Here we take $J^{k+1} - J^k = 10^{-15}$ as a converged solution. The gradient accuracy has been checked for the first and last iteration of the optimization process.

In all the results shown here, except for figure 9, the optimal suction distribution is computed for the whole streamwise computational domain. In figure 9 different control domains are investigated. In all computations, the suction is zero at the first streamwise point to ensure that the original assumption of zero variation of disturbance at X_0 is met.

The relation among the regularization parameter, reduction of disturbance kinetic energy and control energy for all cases is found in the end of this section.

3.1. *Validation and accuracy of the gradient*

The optimization procedure depends on the accuracy of the gradient. If its accuracy is low, then it is less likely to find a minimum and convergence problems will be encountered. Here, we check the accuracy of the gradient by a comparison of the adjoint-based gradients (2.12) with those obtained from a finite-difference approach. The comparison is done by considering a wall-normal velocity perturbation δV_w at $y = 0$. The variation of the functional J with respect to this perturbation is

$$\delta J = \frac{\partial J}{\partial V_\mathrm{w}}\delta V_\mathrm{w}. \quad (3.1)$$

https://doi.org/10.1017/S0022112002001301 Published online by Cambridge University Press

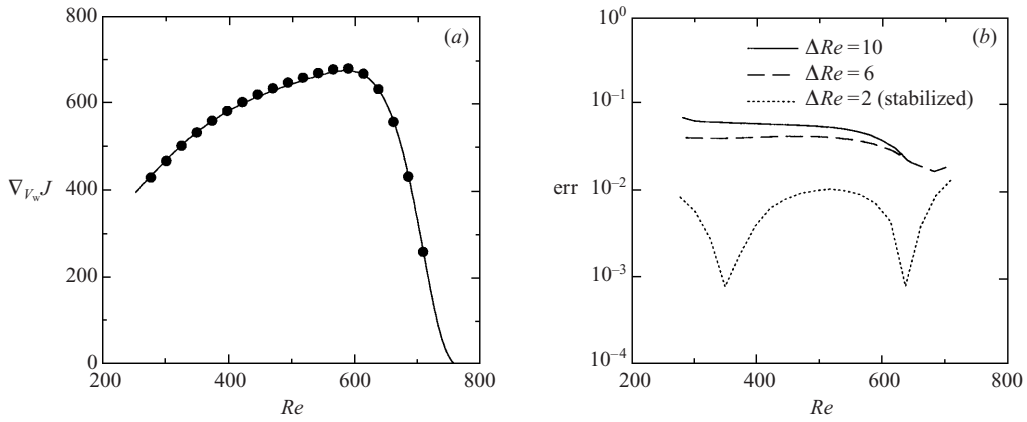


FIGURE 3. Comparison of the gradient from adjoint and central-difference calculations for different streamwise resolution ΔRe. (*a*) $\Delta Re = 2$, the continuous line is the gradient derived from adjoint equations, • marks central-difference calculations. (*b*) The relative error (err) between adjoint and central-difference calculations of the gradient for different streamwise resolution ΔRe.

In the finite-difference approach $\partial J/\partial V_w$ is obtained by using the inhomogeneous wall boundary condition $V_w = \pm\epsilon_w$ at $x = x_n$. The index n refers to the nth streamwise position and ϵ_w is a small positive number. The derivative is then evaluated using a second-order-accurate finite-difference scheme. The discretized expression for δJ in the adjoint approach is given by

$$\delta J = \int_{Z_0}^{Z_1} \left(\sum_{n=2}^{N-1} \nabla_{V_w} J_n \delta V_{w_n} \Delta_n \right) \mathrm{d}z, \tag{3.2}$$

where $\Delta_n = (x_{n+1} - x_{n-1})/2$. In figure 3(*b*), the relative error between $\mathrm{d}J/\mathrm{d}V_w$ and $\nabla_{V_w} J_n \Delta_n$ is compared for different streamwise resolution ΔRe. The calculations are done for a streamwise range $Re = 250$–760 on a quasi-three-dimensional boundary layer where $\mathrm{d}P_e/\mathrm{d}x = 0$, given a T–S wave as the initial disturbance at $x = X_0$. The inviscid flow at $Re = 250$ has an angle of 30°, the non-dimensional spanwise wavenumber $\beta = 0$ and the reduced frequency $F = 2\pi f^\star v_e^\star / U_e^{\star 2} = 10^{-4}$. As can be seen in figure 3(*b*), the relative error decreases as ΔRe is decreased. Here, $\Delta Re = 6$ is the minimum streamwise step size for which the PSE calculations are stable. The values for $\Delta Re = 2$ are computed using the stabilization terms, as explained in § 2.4. In figure 3(*a*), the gradient obtained from the adjoint equations is compared with central-differences when $\Delta Re = 2$ in order to visualize the agreement.

The results presented in this section, had ΔRe chosen such that the relative error (err) was approximately 1%, which required the use of the stabilization procedure. A study was conducted on the influence of changing the streamwise resolution for control of T–S waves in the Blasius boundary layer. It was found that an increased resolution gives a faster convergence and a decrease of the objective function.

3.2. *Two-dimensional boundary layers*

In this section we investigate disturbance control in a two-dimensional boundary layer with zero pressure gradient. The disturbances studied here are chosen to be a T–S wave and/or optimally growing steady streamwise streaks. The initial conditions for T–S waves are taken as the solutions of the local stability theory and the initial condition for the streaks has been calculated using the theory given in Andersson,

https://doi.org/10.1017/S0022112002001301 Published online by Cambridge University Press

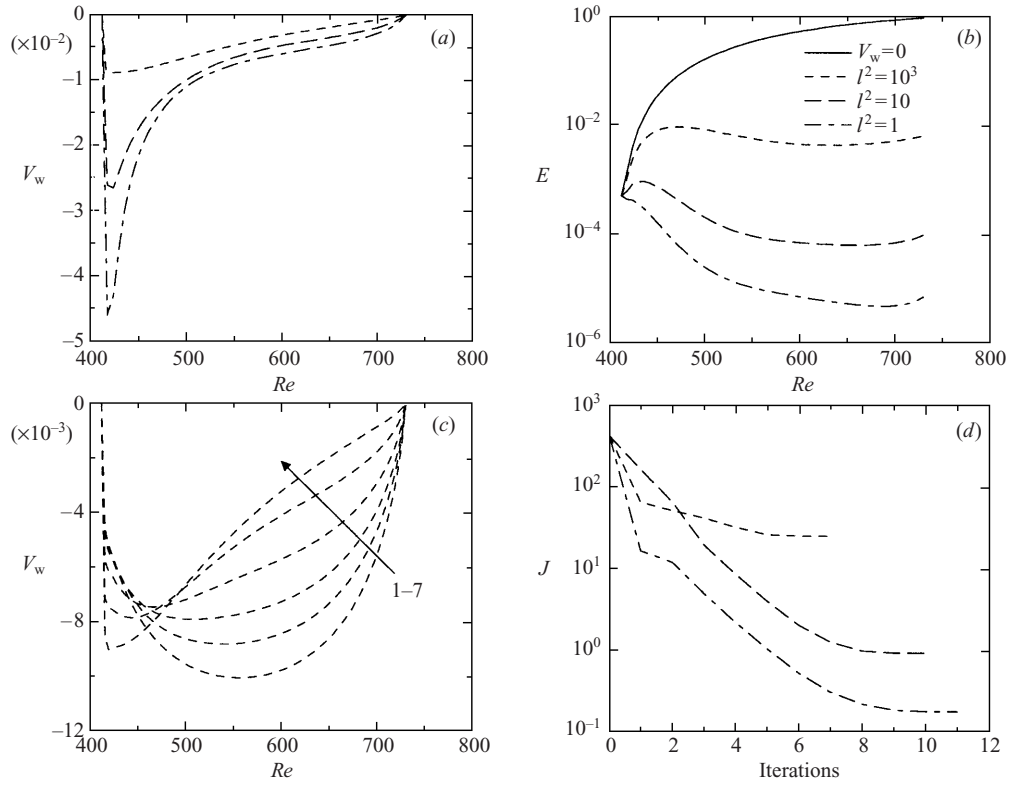


FIGURE 4. Disturbance control of optimally growing steady streamwise streaks in a two-dimensional boundary layer ($dP_e/dx = 0$). The non-dimensional spanwise wavenumber $\beta = 0.292$ at $Re = 412$. Results are shown for $l^2 = 1, 10, 10^3$. (*a*) Optimal suction distributions. (*b*) The disturbance kinetic energy in a mean flow with zero and optimal suction distribution. (*c*) Suction profiles for the different steps in the optimization process, $l^2 = 10^3$. (*d*) The objective function as a function of the iteration step.

Berggren & Henningson (1999). For T–S waves, the streamwise range is chosen such that the unstable region is found between X_0 and X_1. In § 3.2.1 the optimal suction distribution is calculated to control each of these disturbances individually. Here, we also investigate the effect of different domains along the streamwise axis for the control of T–S waves.

The results in this section on control of T–S waves are for a disturbance with a frequency of $F = 10^{-4}$. It is shown that the optimal suction distribution obtained to control the chosen T–S wave has a stabilizing effect on T–S waves with other frequencies. A study has also been performed on the control of T–S waves with both higher and lower frequencies than the one shown here. However, the effect of the optimization process on the growth rate of these disturbances, the corresponding optimal suction profiles and mean flow modifications all show the same behaviour. Thus this choice of frequency gives the general behaviour of the optimization process for a T–S wave instability in a two-dimensional boundary layer.

3.2.1. *Control of single disturbances*

The optimal distribution of suction to control steady streamwise streaks is calculated for a streamwise range $Re = 412$–730. The initial condition which has the

https://doi.org/10.1017/S0022112002001301 Published online by Cambridge University Press

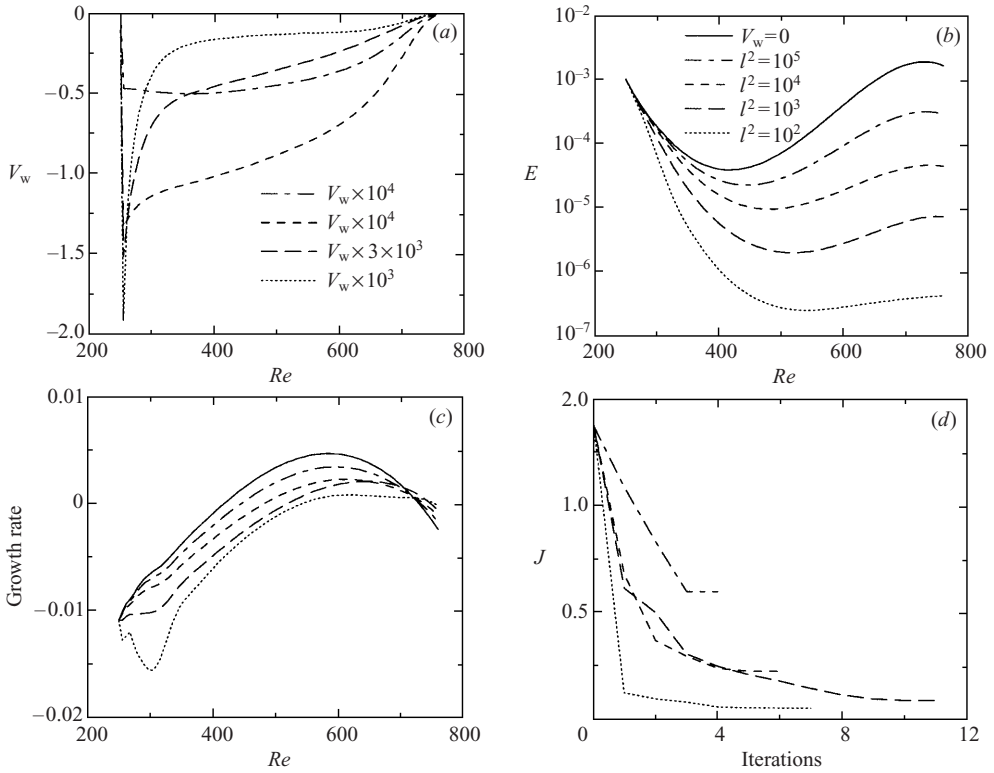


FIGURE 5. Disturbance control of a T–S wave with $F = 10^{-4}$ in a two-dimensional boundary layer ($dP_e/dx = 0$). Results are shown for $l^2 = 10^2,\ 10^3,\ 10^4,\ 10^5$. (*a*) Optimal suction distributions (note the different scalings). (*b*) The disturbance kinetic energy in a mean flow with zero and optimal suction distribution. (*c*) The growth rate, $-\mathrm{Im}(\alpha)$, in a mean flow with zero and optimal suction. (*d*) The objective function as a function of the iteration step.

maximum energy at X_1 is computed using the optimization procedure given in Andersson *et al.* (1999). The non-dimensional spanwise wavenumber $\beta = 0.292$ and the frequency $\omega = 0$. Three test cases are analysed for these parameters in which the regularization parameter l^2 was 1, 10 and 10^3 and the control is applied at $Re = 418$–724. In figure 4(*a*) the optimal suction distributions for all cases are compared. A peak in the suction distribution is seen upstream which becomes more pronounced as the regularization parameter is decreased. In figure 4(*b*) the disturbance kinetic energy of zero and optimal suction are compared. All three suction distributions result in a decrease of the disturbance kinetic energy. However, the main difference between the curves where control is applied is seen in the upstream region. The effect of the optimal suction distributions given in figure 4(*a*) is that the damping of the disturbance kinetic energy is increased in the upstream region as l^2 is decreased. Figure 4(*c*) illustrates the changes in the suction distribution during the optimization procedure. Here, V_w is plotted for each iteration in the optimization loop for the case with $l^2 = 10^2$. The optimal distribution is found after 7 iterations. The difference between the sixth and seventh iteration cannot be distinguished. In figure 4(*d*) the objective function is given as function of the iteration number for all cases to illustrate the convergence of the optimization procedure.

The optimal distribution of suction to control T–S wave instabilities is calculated for a streamwise range $Re = 250$–760. The first investigation compares different

https://doi.org/10.1017/S0022112002001301 Published online by Cambridge University Press

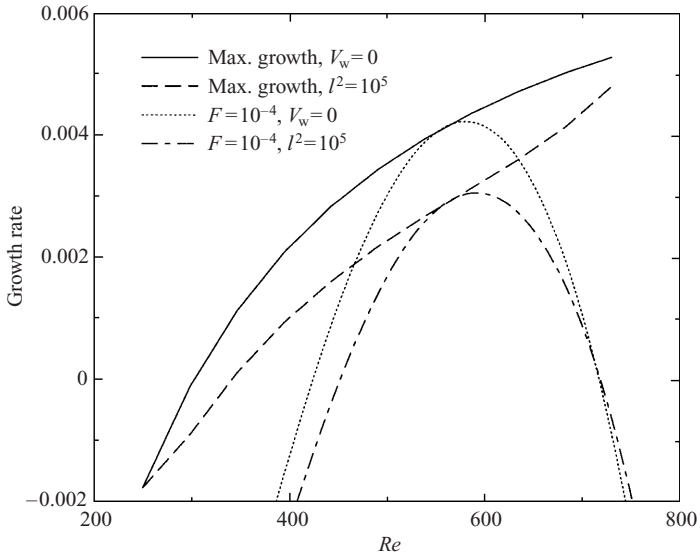


FIGURE 6. Maximum local growth rate compared with local growth rate of a T–S wave with $F = 10^{-4}$, for zero and optimal suction in a two-dimensional boundary layer ($dP_e/dx = 0$). The optimal suction is computed for control of a T–S wave with $F = 10^{-4}$ given that $l^2 = 10^5$ for a streamwise range $Re = 250$–760. Calculations of maximum local growth rate are made with $\Delta F = 2.5 \times 10^{-6}$.

regularization parameters, here $l^2 = 10^2$, 10^3, 10^4, 10^5 while control is applied at $Re = 256$–754. The results can be seen in figure 5. In figure 5(a) the optimal suction distributions from all cases are compared. The optimal suction distribution tends to peak upstream as the penalty on the control is reduced, and this peak is upstream of the unstable region for all cases. Even though the magnitude of the suction rates is within the original assumptions, one should also note that a decreased penalty on the control produces suction distributions with large streamwise variations in the upstream domain. At the point where our results show a peak they are thus locally outside the range of validity of the parabolic theory employed, since the gradient of the control velocity at the initial control point approaches infinity as the step size in the streamwise direction approaches zero. In figure 5(b) the disturbance kinetic energy is compared for zero and optimal suction distribution. A reduction of disturbance kinetic energy can be observed as the penalty of the control is reduced. The growth rate for all cases is given in figure 5(c). In all cases the growth rate is decreased as l^2 is decreased and the reduction is more pronounced in the upstream region. Finally, in figure 5(d) the objective function is plotted as a function of the iteration number to show the convergence of the optimization procedure.

A question that arises is whether the suction distribution which is optimal for one chosen T–S wave will damp or amplify other instability waves in the chosen streamwise domain. This is analysed by computing the maximum local growth rate, i.e. local growth rate over all possible frequencies, at a number of streamwise positions both with zero and the optimal suction distribution. The streamwise range and optimal suction distribution are taken from figure 5 with $l^2 = 10^5$. The results are shown in figure 6 where the maximum local growth rate has been computed for $\Delta F = 2.5 \times 10^{-6}$ and $\Delta Re = 50$ as the reduced frequency and streamwise resolution respectively. Here, it is shown that the optimal suction distribution for one given frequency has a

https://doi.org/10.1017/S0022112002001301 Published online by Cambridge University Press

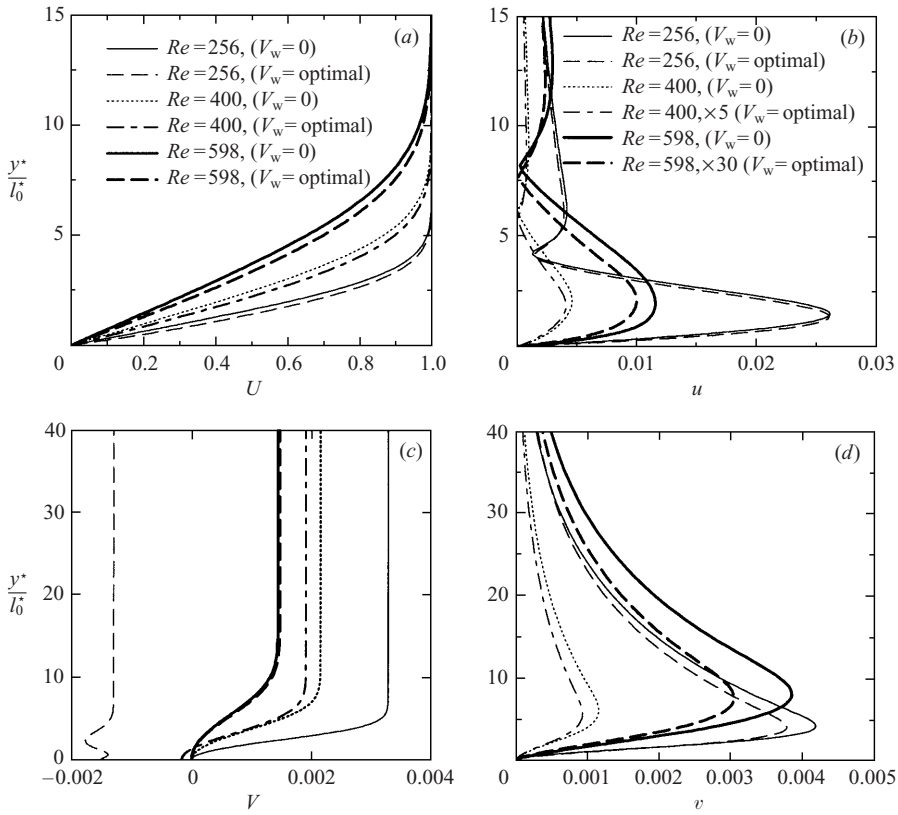


FIGURE 7. Modification of the two-dimensional mean flow ($dP_e/dx = 0$) and disturbance velocity due to optimal suction computed to control a T–S wave with $F = 10^{-4}$ when $l^2 = 10^2$ in a streamwise range $Re = 250$–760. Results are presented for $Re = 256$, 400, 598. (*a*) Streamwise and (*c*) wall-normal velocity of the mean flow subject to zero and optimal suction. Absolute value of the (*b*) streamwise and (*d*) wall-normal disturbance velocity (note the different scalings).

stabilizing effect on all other frequencies in the given streamwise range. Further, the local growth rate for the T–S wave with $F = 10^{-4}$ has been plotted both with zero and optimal suction distribution. The result shows that the chosen disturbance corresponds to the maximum growth rate both with zero and optimal suction at a given streamwise position.

The effect of imposing suction at the wall is that the velocity profile of the mean flow becomes fuller, which is known to stabilize the viscous instability waves. In figure 7 the effects on the streamwise and wall-normal velocity components of the mean flow are shown for three different streamwise positions. The streamwise and wall-normal disturbance velocity components are also plotted. The suction distribution is that of figure 5 for $l^2 = 10^2$. The first position, $Re = 256$, is close to X_0, the second position $Re = 400$ is close to where the disturbance starts to grow and the last position $Re = 598$ is roughly halfway into the unstable region. In figure 7(*a*) the streamwise velocity profile is plotted for these three positions, when zero and optimal suction are applied. In all three cases the mean flow profiles have become fuller (or thickened). It should be noted that even though the optimal suction distribution shows a significant peak in the vicinity of $Re = 256$, see figure 5(*a*), the effect on the streamwise mean velocity is not large. The effect of suction on the mean flow is instead more pronounced

https://doi.org/10.1017/S0022112002001301 Published online by Cambridge University Press

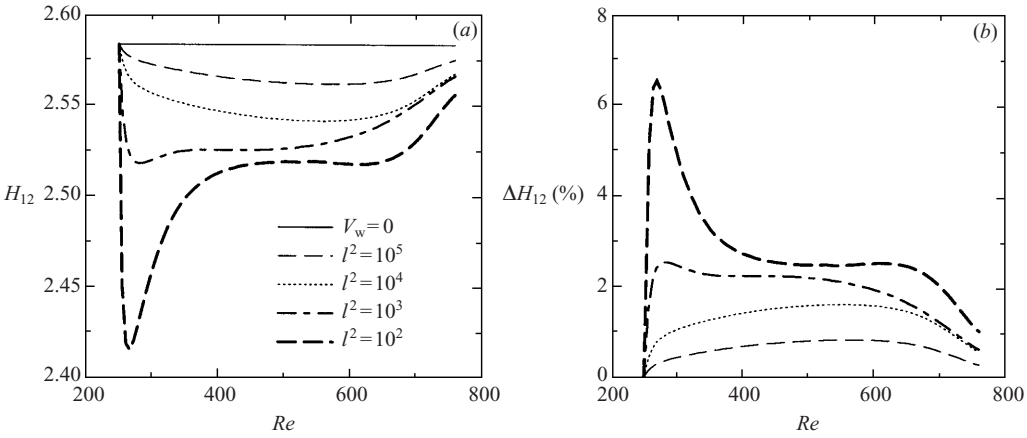


FIGURE 8. Shape factor (H_{12}) for control of a T–S wave with $F = 10^{-4}$ in a two-dimensional boundary layer ($dP_e/dx = 0$). Results are shown for $l^2 = 10^2, 10^3, 10^4, 10^5$ (a) Shape factor. (b) Relative change in the shape factor (ΔH_{12}) in percent, between controlled and uncontrolled case.

for the wall-normal component, see figure 7(c), especially in the upstream region. The amplitudes of the streamwise and wall-normal disturbance velocities are shown for the cases of zero and optimal suction in figures 7(b) and 7(d), respectively. The initial condition is the same for zero and optimal suction and the effect of suction on both components is similar. At the upstream position, the variation due to suction is small. The results at the most downstream position show a larger reduction of disturbance amplitude. Here, the results for the case of optimal suction at $Re = 400$ and 598 are magnified to make the shape visible. In all cases the disturbance shape is the same as the optimal suction distribution is applied but the magnitude is decreased. Further, the peak velocity is moved somewhat closer to the wall due to the decreased boundary layer thickness.

As pointed out in the introduction, the mean flow pressure distribution is assumed to be unchanged by the applied suction. If this were not the case, then an additional set of equations would be needed in order to solve for the exterior pressure distribution in the optimization process. In order to gain some insight into this, the shape factor H_{12} (displacement thickness/momentum thickness) is plotted in figure 8(a) for all cases in figure 5. In figure 8(b) the relative change of H_{12} between the controlled and uncontrolled case is plotted. For the three cases $l^2 = 10^3,\ 10^4,\ 10^5$, the difference in shape factor ranges between 0.5% and 2%. However, for the case of $l^2 = 10^2$ a peak of 6% difference appears in the upstream region. Note, that all cases have maximum suction velocities which are smaller than the original assumption of $V_w \sim O(1/Re)$.

Figure 9 illustrates the effects of changing the size and location of the control domain. Here, the same case as in figure 5 with $l^2 = 10^3$ is used. Three different control regions are compared. In the first case, the control is applied to $Re = 412$–554 which is from the initial point of the unstable region (branch I of the neutral stability curve) to roughly halfway into the unstable region. In the second case, $Re = 412$–718, the control domain is extended over the whole unstable region and in the last case, $Re = 256$–754, the control is applied over the whole computational domain. The corresponding optimal suction velocity profiles can be seen in figure 9(a). Results for all cases show a suction peak in the upstream region of the control domain. In figure 9(b) the kinetic disturbance energy is shown for all cases. The first case shows a significant reduction of energy as the control is applied but continues to grow when

https://doi.org/10.1017/S0022112002001301 Published online by Cambridge University Press

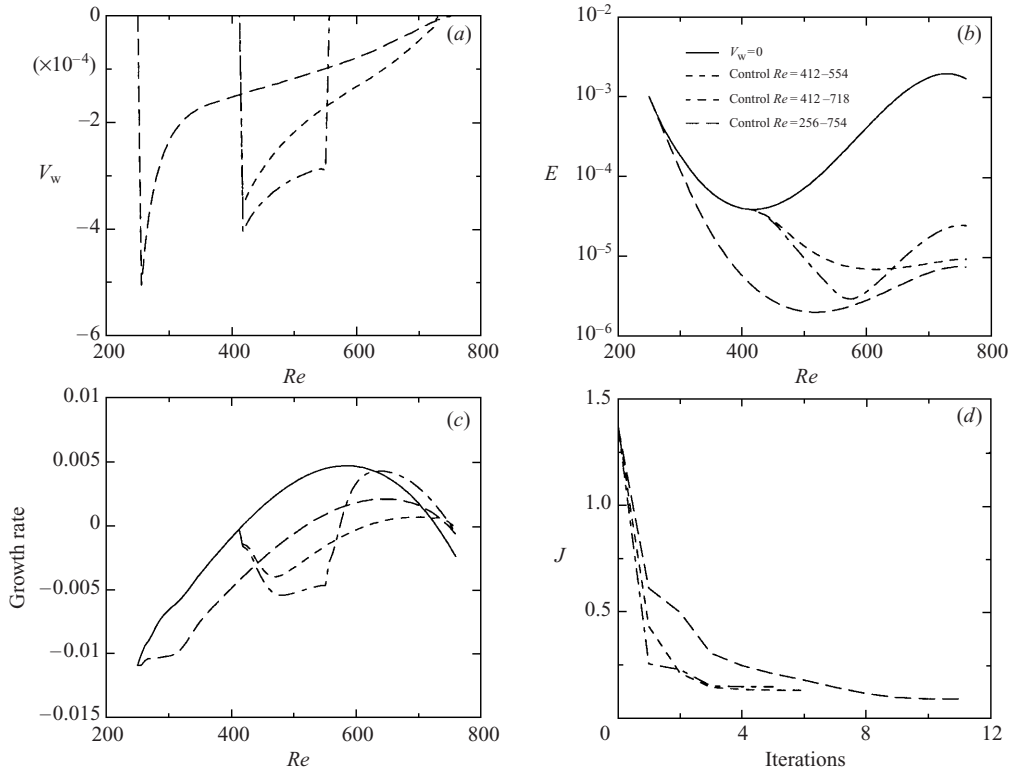


FIGURE 9. Disturbance control of a T–S wave with $F = 10^{-4}$ in a two-dimensional boundary layer ($dP_e/dx = 0$). Results are presented for different control domains given that $l^2 = 10^3$. (*a*) Optimal suction distributions. (*b*) The disturbance kinetic energy in a mean flow with zero and optimal suction. (*c*) The growth rate, $-\mathrm{Im}(\alpha)$, in a mean flow with zero and optimal suction. (*d*) The objective function as a function of the iteration step.

the control is turned off. The second and last cases show that approximately the same reduction of energy at the final streamwise position can be obtained either by acting only in the unstable region or in the whole domain. The growth rate is given in figure 9(*c*). In the first and second cases, the growth rate follows the curve of zero suction until the control is turned on. A large reduction in growth rate can then be seen in the upstream region of the control domain. The first case shows a significant increase as the control is turned off inside the unstable region. In figure 9(*d*) the objective function is plotted as a function of the iteration number to visualize the convergence of the optimization procedure.

3.2.2. *Control of multiple disturbances*

The theory in § 2.3 was introduced to account for more than one disturbance in the domain. This will produce an optimal suction profile that reduces the disturbance kinetic energy for all disturbances accounted for. Here, we analyse two disturbances, a T–S wave and optimally growing streamwise steady streaks, with an initial energy such that they give the same maximum disturbance energy at the downstream position X_1. The domain is chosen so that X_0 and X_1 are at the first and second branches of the neutral stability curve for the T–S wave with $F = 10^{-4}$. The initial condition for the steady streaks is computed using the optimization technique given in Andersson *et al.* (1999) to provide the maximum growth at X_1 for the chosen domain. In all calcula-

https://doi.org/10.1017/S0022112002001301 Published online by Cambridge University Press

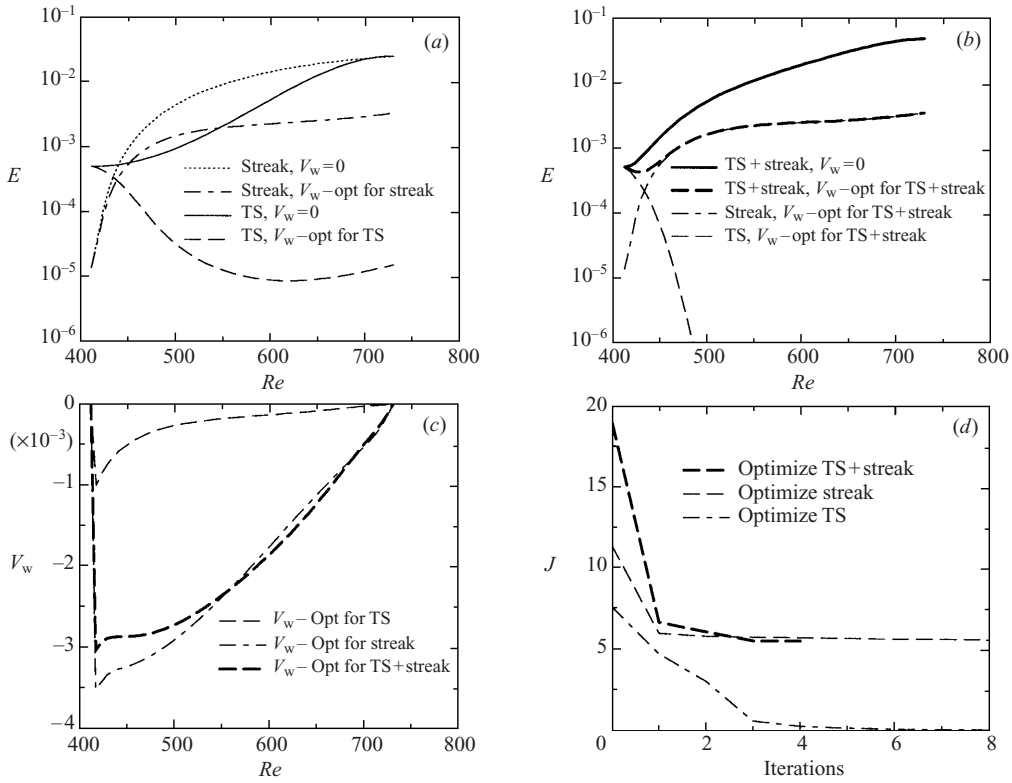


FIGURE 10. Control of two disturbances in a two-dimensional boundary layer ($dP_e/dx = 0$). The disturbances are a T–S wave ($F = 10^{-4}$) and optimally growing streamwise streaks ($\beta = 0.292$ at $Re = 412$) and $l^2 = 10^3$. Disturbance kinetic energy in a mean flow with zero and optimal suction: (*a*) the suction distribution is computed for each disturbance separately, (*b*) the suction distribution is computed to account for both disturbances (see § 2.3). (*c*) Optimal suction distributions. (*d*) The objective function as a function of the iteration step.

tions $l^2 = 10^3$ which means that the same weighting is given between the disturbance and control energy in all cases. The optimal suction profile was first computed for each of the disturbances individually. A comparison of the disturbance kinetic energy for zero and the corresponding optimal suction can be seen in figure 10(*a*). It is shown that the reduction of kinetic energy is more than two decades larger for the T–S wave as the optimal control is applied. Given the same l^2, it is therefore possible to say that optimally growing streamwise streaks demand a stronger control than T–S waves. The corresponding suction distributions can be seen in figure 10(*c*). It can be seen in this comparison that the magnitude of the control of steady streaks is larger than for T–S waves. This is expected however, as the total disturbance kinetic energy of the streaks is larger than that of the T–S wave given that the energy is the same at X_1, see figure 10(*a*), and therefore should result in a larger control energy. Then, the optimal suction profile was calculated for the sum of both disturbances using (2.22) with $l^2 = 10^3$. In figure 10(*b*), the disturbance kinetic energy is shown when the optimal control for the sum of both disturbances is applied to each disturbance individually and the sum of both disturbances. The corresponding optimal suction distribution can be seen in figure 10(*c*). Here, the total kinetic energy for the streaks is larger than for the T–S wave, and the control will act primarily on the streaks. Therefore,

https://doi.org/10.1017/S0022112002001301 Published online by Cambridge University Press

the optimal suction distribution for the sum of the disturbances is similar to that of the streaks. When the optimal suction profile for the sum is used on the T–S wave then the energy decreases further and drops to 10^{-11}, out of range in figure 10(*b*), at the downstream position X_1. This is 5 decades lower than the optimal suction profile for control of just the T–S wave gives. In figure 10(*d*) the objective function is given as a function of the iteration number to show the convergence of the optimization process.

3.3. *Three-dimensional boundary layers*

Here, we study the control of three-dimensional disturbances in quasi-three-dimensional boundary layers subjected to a pressure gradient. In the first case, the flow is subjected to an adverse pressure gradient and the disturbance parameters have been chosen such that it has the maximum growth rate (over all F and β) at some position in the computational domain. Further studies have been performed on control of oblique waves with other frequencies and spanwise wavenumbers than the one shown here. The behaviour of the optimal suction distributions, mean flow and disturbances are similar. Therefore, we find that the disturbance parameters chosen here represents the general behaviour of the optimization process and results. In the second case, control is presented for a steady cross-flow mode in a mean flow with a favourable pressure gradient where we have chosen the case from Högberg & Henningson (1998). Although the stationary cross-flow modes are not the most amplified ones, in the presence of surface roughness they are often the dominant disturbances.

3.3.1. *Control in a flow with an adverse pressure gradient*

The control of an oblique wave is analysed in a quasi-three-dimensional incompressible boundary layer with an adverse pressure gradient ($U_e = (x/x_0)^{-0.05}$). The streamwise range is $Re = 250$–760, the non-dimensional spanwise wavenumber $\beta = -0.02$ and the reduced frequency $F = 10^{-4}$. The inviscid flow at $Re = 250$ has an angle of 45° and the control has been applied at $Re = 256$–754. In this case l^2 has been altered to compare the impact of different regularization parameters on the control energy used. The results comparing various l^2 can be seen in figure 11. In figure 11(*a*) the optimal suction distribution V_w is plotted. A suction peak appears at an upstream position of the control domain and is more pronounced as l^2 is decreased. Downstream of the suction peak the suction distribution is nearly constant before it finally decreases to zero. It is evident from this figure that a decreased penalty on the control will concentrate the increased control effort in the upstream domain. This creates, as in figure 5, a strong streamwise variation of the suction distribution in this region. The disturbance kinetic energy is compared in figure 11(*b*) for the cases of zero and optimal suction distribution. A reduction of kinetic energy is observed in all cases, starting in the upstream region of the control domain. Further, the reduction is increased as l^2 is decreased. In figure 11(*c*) the growth rate is compared for zero and optimal suction distribution and it is shown that the growth rate is decreased as l^2 is decreased. Note that the growth rate for the case with $l^2 = 10^2$ shows a strong streamwise variation in the upstream domain. In figure 11(*d*) the objective function is plotted for each iteration in the optimization loop to demonstrate the convergence of the optimization process.

In this analysis only one oblique wave has been considered. The effects on the growth rate of other oblique waves are investigated using the suction distribution

https://doi.org/10.1017/S0022112002001301 Published online by Cambridge University Press

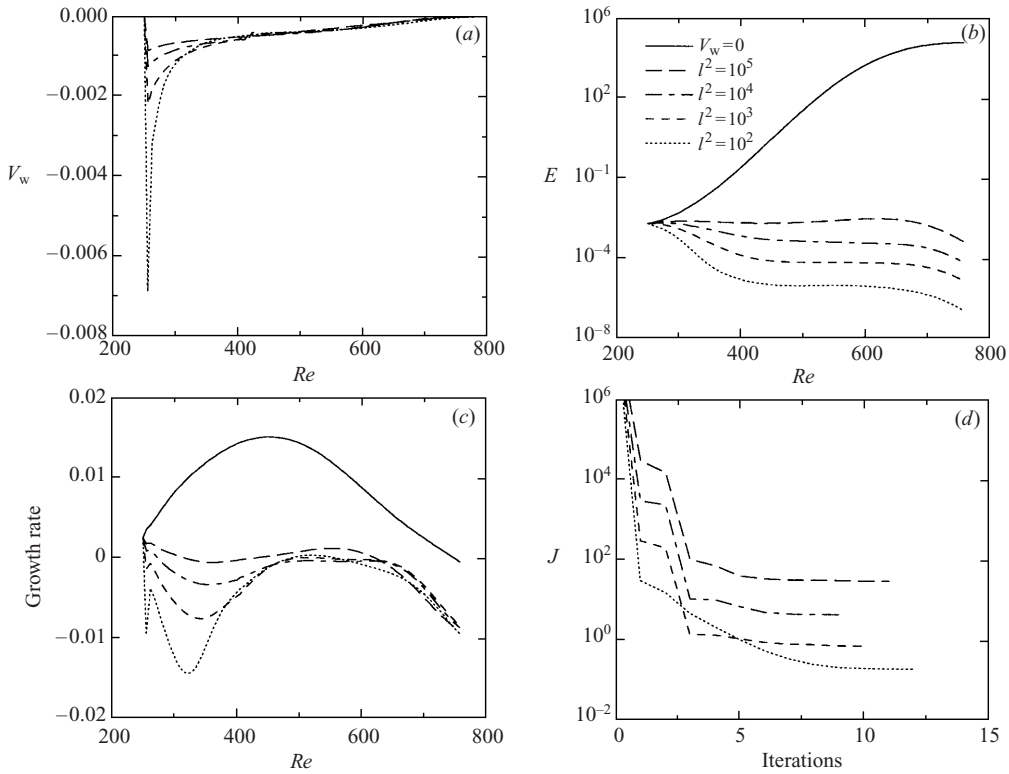


FIGURE 11. Control of an oblique wave in a three-dimensional boundary layer with an adverse pressure gradient ($U_e = (x/x_0)^{-0.05}$). The inviscid flow at $Re = 250$ has an angle of 45° and the non-dimensional spanwise wavenumber $\beta = -0.02$. Results are shown for $l^2 = 10^2, 10^3, 10^4, 10^5$. ($a$) Optimal suction distributions. (b) The disturbance energy in a mean flow with zero and optimal suction. (c) The growth rate, $-\mathrm{Im}(\alpha)$, in a mean flow with zero and optimal suction. (d) The objective function as a function of the iteration step.

from the analysis above with $l^2 = 10^2$. This is done by computing the local growth rate in the (F, β) plane at two different streamwise positions. Contours of the local growth rate are given in figure 12 where the thick contours mark zero growth rate and the • marks the oblique wave analysed in figure 11. Note here that the reduced frequency F, the non-dimensional spanwise wavenumber β and the growth rate are scaled with the reference values taken at X_0. Figure 12(a) shows the local growth rate for oblique waves at $Re = 418$ with zero suction. Here it is shown that the disturbance analysed in figure 11 is close to the maximum growth rate for all oblique waves at this streamwise position. No figure is shown for the case when optimal suction is applied as all waves are damped at this position. The result in figure 12(b, c) correspond to $Re = 676$ with the mean flow subjected to zero and optimal suction respectively. The optimal suction is shown to make all oblique waves more stable. However, the effect is less than in the upstream region.

It is also of interest to see how the inflection point due to the adverse pressure gradient is affected by the optimal suction. The suction distributions shown in figure 11(a) are similar except for the upstream region. Therefore, the case of figure 11 with $l^2 = 10^5$ is chosen to see if the smallest amount of suction still affects the inflection point of the mean flow. The results for two different streamwise positions are seen in

https://doi.org/10.1017/S0022112002001301 Published online by Cambridge University Press

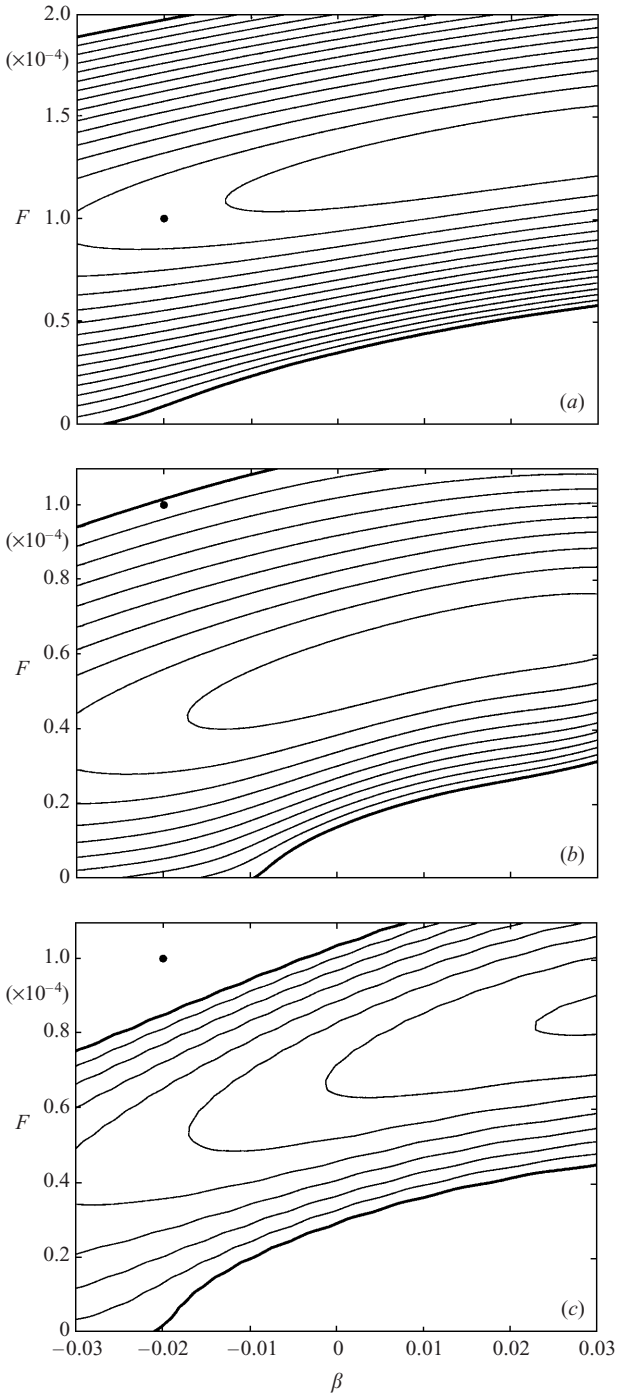


FIGURE 12. Contours of local growth rate at different streamwise positions in a flow with an adverse pressure gradient ($U_e = (x/x_0)^{-0.05}$). The inviscid flow at $Re = 250$ has an angle of 45°. (*a*) At $Re = 418$ with zero suction (all disturbances are damped using optimal suction at this position). (*b*) At $Re = 676$ with zero suction. (*c*) At $Re = 676$ with an optimal suction distribution given by the case in figure 11 where $l^2 = 10^2$. Here F, β and the local growth rate are scaled with reference values at X_0. The thick contours denote zero growth rate and the contour spacing is 0.0005. The • marks the disturbance initial condition used in figure 11.

https://doi.org/10.1017/S0022112002001301 Published online by Cambridge University Press

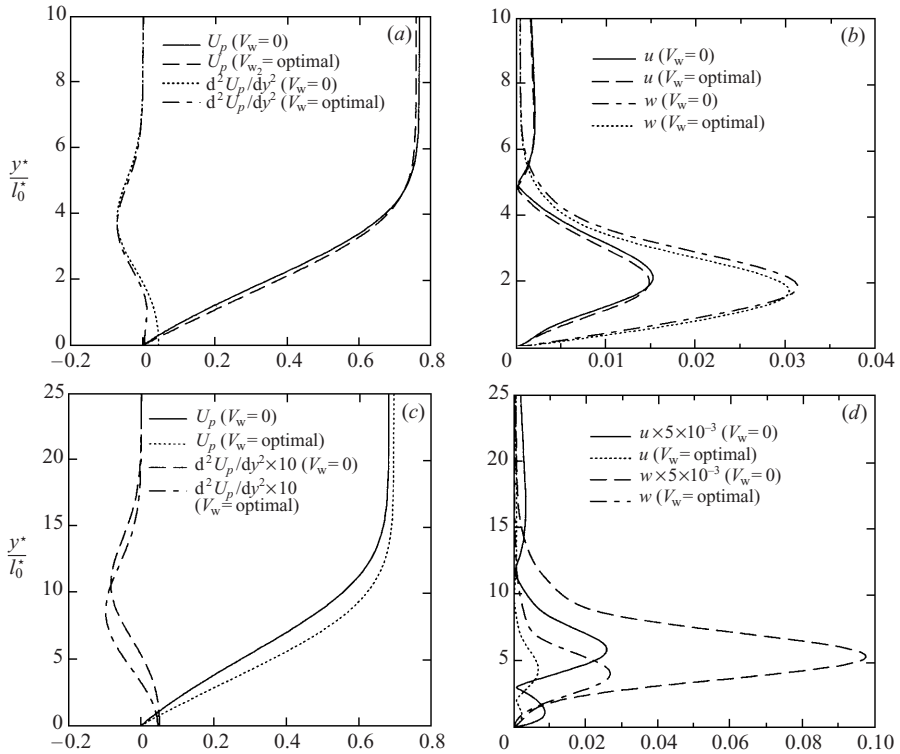


FIGURE 13. Modification of the three-dimensional mean flow with an adverse pressure gradient ($U_e = (x/x_0)^{-0.05}$) and disturbance velocity, due to optimal suction ($l^2 = 10^5$). The inviscid flow at $Re = 250$ has an angle of 45° and the control is computed for an oblique wave ($F = 10^{-4}$, $\beta = -0.02$ at $Re = 250$) between $Re = 250$ and 760. $U_p = (\alpha_r U + \beta W)/k$ and the absolute value of the streamwise and spanwise disturbance velocity are denoted u and w respectively. The streamwise positions are: $Re = 262$ in (a, b) and $Re = 694$ in (c, d).

figure 13. Here the mean flow has been projected in the direction of the wavenumber vector $\boldsymbol{k}$, with absolute value $k = (\alpha^2 + \beta^2)^{1/2}$, and is given as $U_p = (\alpha U + \beta W)/k$. In figure 13($a$) U_p and its corresponding second wall-normal derivative are shown at $Re = 262$. The effect of the optimal suction is small but increases the velocity inside the boundary layer. The plot of the second wall-normal derivative of U_p shows that the inflection point has almost disappeared. The effect on the disturbance velocities due to the mean flow modification at $Re = 262$ is shown in figure 13(b). Here, the absolute value of the streamwise and spanwise disturbance velocities are plotted. Both components have maintained their shape but the maximum values are decreased and moved towards the wall. The quantities in figure 13(a, b) are plotted at $Re = 694$ in figure 13(c, d) respectively. At this streamwise position all suction distributions shown in figure 11(a) are similar and therefore are the mean flow modifications at this position similar for all cases shown in figure 11. The mean flow components shown in figure 13(c) have become fuller. However, the inflection point of the streamwise component does still exist but has moved towards the wall. The maximum values of the disturbance velocities shown in figure 13(d) have moved closer to the wall and decreased by a factor of 10^3. Further, it is noted that the disturbance shape has been maintained here also.

https://doi.org/10.1017/S0022112002001301 Published online by Cambridge University Press

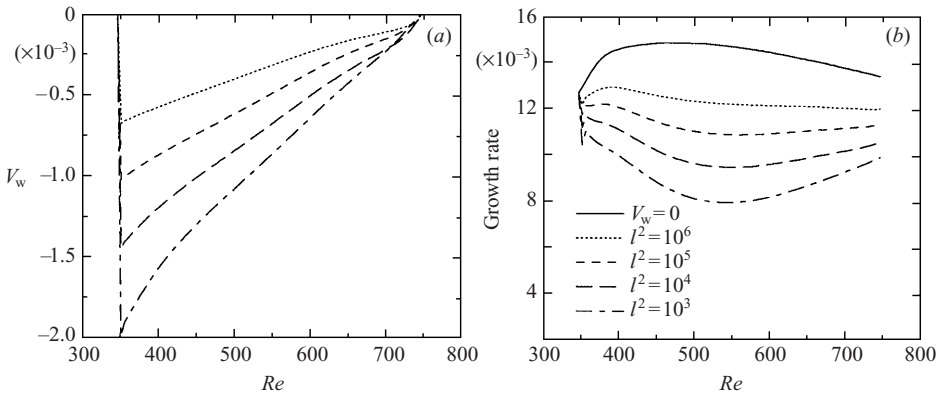


FIGURE 14. Control of a stationary cross-flow mode in a three-dimensional boundary layer with a favourable pressure gradient ($U_e = (x/x_0)^{0.34207}$). The inviscid flow at $Re = 346$ has an angle of 55.26° and the non-dimensional spanwise wavenumber $\beta = -0.256$. Results are presented for $l^2 = 10^3, 10^4, 10^5, 10^6$. (*a*) Optimal suction distributions. (*b*) Growth rate $-\mathrm{Im}(\alpha)$.

3.3.2. *Control in a flow with a favourable pressure gradient*

The control of a steady cross-flow mode is analysed in a quasi-three-dimensional incompressible boundary layer with a favourable pressure gradient taken from Högberg & Henningson (1998) ($U_e = (x/x_0)^{0.34207}$). The streamwise range is $Re = 346$–746 and the inviscid flow at $Re = 346$ has an angle of 55.26°. Here, the control has been applied at $Re = 351$–741. The initial condition of the disturbance is taken as the local solution at $Re = 346$ where the non-dimensional spanwise wavenumber is $\beta = -0.256$.

In figure 14 results are presented for the optimization with different values of the regularization parameter l^2. Here, $l^2 = 10^3$ gives a maximum suction velocity which is close to the maximum value for which the boundary layer equations are valid (see § 2.1.1). The optimal suction distributions due to the variation of l^2 are shown in figure 14(*a*). As l^2 is decreased the magnitude of the suction velocity is increased. The maximum of the suction velocity is found in the upstream region in all cases but does not appear as a pronounced peak as was shown in § 3.2 and § 3.3.1.

The corresponding growth rates for zero and optimal suction are presented in figure 14(*b*). The uncontrolled steady cross-flow mode studied here has a positive growth rate in the whole domain and it is shown here that the optimal suction reduces the growth rate. However, not even the largest magnitude of steady optimal suction, i.e. the smallest l^2, can stabilize the cross-flow mode. The largest reduction of growth rate is found at approximately the same streamwise position regardless of l^2 and it should be noted that this is far downstream of the point where suction has its maximum.

The results shown in this section have not been computed given a certain amount of control energy. Instead, the regularization parameter l^2, given in (2.9), has been used to balance the measured disturbance kinetic energy and the control energy. In practice this means that increasing l^2 will decrease the available control energy and vice versa in the optimization process. In an application of this theory it might be of interest to see how the benefit (reduction in disturbance kinetic energy) is related to a certain amount of control energy. This can be seen in figure 15(*a*) for all cases studied in this section. Here, the benefit is given as the ratio between

https://doi.org/10.1017/S0022112002001301 Published online by Cambridge University Press

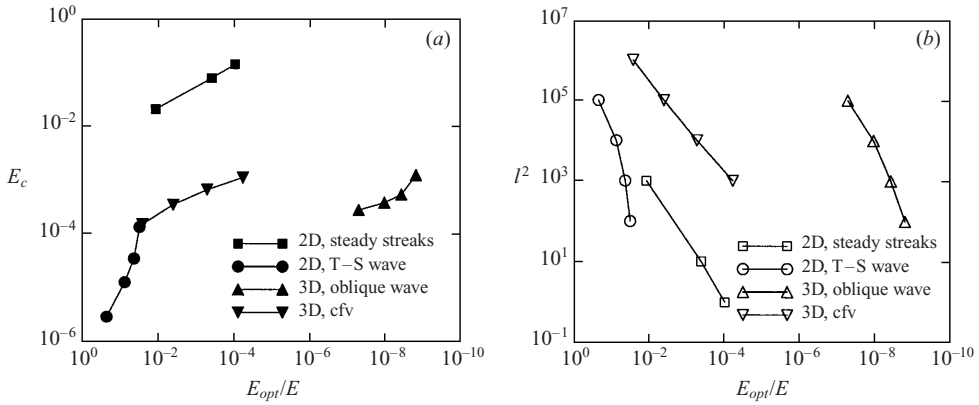


FIGURE 15. Relation between reduction in disturbance kinetic energy and (*a*) optimal control energy E_c, (*b*) the regularization parameter l^2. Here E_{opt} and E are the disturbance kinetic energies given optimal and zero suction respectively.

the disturbance kinetic energies for optimal and zero suction denoted as E_{opt} and E, respectively. The corresponding relation between l^2 and the benefit is given in figure 15(*b*).

4. Discussion and conclusions

A procedure to control disturbances in quasi-three-dimensional incompressible boundary layers on a flat plate has been derived and analysed. Here, disturbances are controlled by modifying the mean flow using the wall-normal velocity component of the mean flow on the wall. The optimization procedure is gradient based and the aim is to minimize an objective function balancing a measure of the state and the control energy. The gradient is derived using adjoint equations and the coupling between the adjoint of the PSE (APSE) and the adjoint of the boundary layer equations (ABLE) is shown. The measure of the state is the disturbance kinetic energy in the whole domain and here it has been generalized to account for more than one disturbance.

To increase the streamwise resolution, a stabilization procedure has been used for the PSE which modifies both the APSE and the ABLE. The gradients derived using the adjoint equations have been validated with a finite-difference approach and it has been shown that the gradient accuracy is increased as the streamwise resolution is increased. A finite-difference check has also been continuously done on the final gradients in the optimization, indicating that the continuous approach used for the derivation of the adjoint equations has been adequate.

Numerical results have been presented for disturbance control in both two- and quasi-three-dimensional incompressible boundary layers. The results shown for suction distributions have a similar shape for control of T–S wave instabilities and steady optimally growing streamwise streaks in two-dimensional boundary layers and oblique waves in quasi-three-dimensional boundary layers. The suction profiles tend to peak close to the first point of the computational domain but become significantly smaller and nearly constant further downstream. This tendency become more pronounced as the penalty of the control l^2 is reduced, i.e. the freedom of the control is increased. Although the magnitudes of the suction distributions are $V_w \sim O(Re^{-1})$, care must be taken as a decrease in l^2 may result in large streamwise variations of both V_w and the growth rate. Care must be taken so that this variation is small enough not to

https://doi.org/10.1017/S0022112002001301 Published online by Cambridge University Press

contradict the underlying hypothesis of a slow streamwise variation assumed in both the BLE and PSE.

If solutions without sharp peaks are desired then additional terms can be added to the objective function in which a penalty is put on for example the streamwise derivative of the control variable. This procedure has been used in shape optimization problems, for example, where the goal has been to create not only an optimal geometry but also with a certain degree of smoothness. Such constraints are not investigated here as they are more connected to user applications and an extension of the optimal control theory rather than the methodology itself.

In both two- and quasi-three-dimensional boundary layers it has been shown that the boundary layer velocity profiles have become fuller as the optimal suction distribution is applied. Both of these observations show that the stabilization obtained by the suction distribution is a modification of the mean flow similar to that of a flow with a favourable pressure gradient with zero suction. The relation between the suction velocity, pressure gradient and second wall-normal derivative of the streamwise velocity on the wall is understood by looking at (2.2) for $y = 0$:

$$V_{\mathrm{w}}\frac{\partial U}{\partial y} + \frac{\mathrm{d}P_e}{\mathrm{d}x} = \frac{1}{Re}\frac{\partial^2 U}{\partial y^2}. \tag{4.1}$$

In the case of a Blasius mean flow ($\mathrm{d}P_e/\mathrm{d}x = 0$), the right-hand side of (4.1) gives the favourable pressure gradient which corresponds to a certain suction velocity. However, in the case of an adverse pressure gradient ($\mathrm{d}P_e/\mathrm{d}x > 0$), the modification is dependent on the magnitude of the suction velocity as neither of the two terms on the left-hand side of (4.1) is zero. Here, a favourable pressure gradient is only obtained if $V_{\mathrm{w}}\partial U/\partial y < \mathrm{d}P_e/\mathrm{d}x$. A stabilizing effect will still occur if $V_{\mathrm{w}}\partial U/\partial y > \mathrm{d}P_e/\mathrm{d}x$ but the location of the inflection point due to the adverse pressure gradient will be dependent on the magnitude of V_{w}.

As a result of the optimal suction distribution, the disturbance kinetic energy is decreased as the control energy is increased (here shown by decreasing l^2). For control of T–S waves in two-dimensional boundary layers and oblique waves in quasi-three-dimensional boundary layers, the growth rate has the largest decrease in the upstream domain when l^2 is decreased. This corresponds to where the optimal suction has its peak. When control is applied to the steady cross-flow mode, the largest decrease in growth rate is at the same streamwise location independent of l^2. Further, this is far downstream of the point where the suction has its maximum. For T–S wave instabilities in the Blasius flow it has been shown that essentially the same energy reduction at the last streamwise point is achieved when the control is applied in the whole unstable region compared to control which starts just upstream and ends just downstream of the unstable region.

One of the assumptions made in this analysis is that the disturbances have homogeneous boundary conditions at the wall and therefore no coupling to the mean flow at the wall. This can be interpreted as uniform suction through a porous material. The validity of these boundary conditions should be analysed if instead discrete holes are used.

J. O. P. acknowledges the Swedish Foundation for Strategic Research (SSF) who has financed this work through the Integral Vehicle Structure (IVS)-program.

https://doi.org/10.1017/S0022112002001301 Published online by Cambridge University Press

Appendix A. Matrices of the PSE

The matrices $\boldsymbol{A},\boldsymbol{B},\boldsymbol{C}$ and $\boldsymbol{D}$ in the PSE are

$$\boldsymbol{A}=\begin{bmatrix} \mathrm{i}\alpha & 0 & \mathrm{i}\beta & 0 \\ \xi+\dfrac{\partial U}{\partial x} & \dfrac{\partial U}{\partial y} & 0 & \mathrm{i}\alpha \\ 0 & \xi+\dfrac{\partial V}{\partial y} & 0 & 0 \\ \dfrac{\partial W}{\partial x} & \dfrac{\partial W}{\partial y} & \xi & \mathrm{i}\beta \end{bmatrix}, \quad \boldsymbol{B}=\begin{bmatrix} 0 & 1 & 0 & 0 \\ V & 0 & 0 & 0 \\ 0 & V & 0 & 1 \\ 0 & 0 & V & 0 \end{bmatrix},$$

$$\boldsymbol{C}=\begin{bmatrix} 0 & 0 & 0 & 0 \\ -\dfrac{1}{Re} & 0 & 0 & 0 \\ 0 & -\dfrac{1}{Re} & 0 & 0 \\ 0 & 0 & -\dfrac{1}{Re} & 0 \end{bmatrix}, \quad \boldsymbol{D}=\begin{bmatrix} 1 & 0 & 0 & 0 \\ U & 0 & 0 & 1 \\ 0 & U & 0 & 0 \\ 0 & 0 & U & 0 \end{bmatrix},$$

where

$$\xi=-\mathrm{i}\omega+\mathrm{i}\alpha U+\mathrm{i}\beta W+\frac{1}{Re}(\alpha^2+\beta^2).$$

Appendix B. Derivation of adjoint equations

The gradient of the objective function, J, with respect to the wall-normal velocity component of the mean flow on the wall, V_{w}, is derived using the APSE and the ABLE. The question is whether to use a 'discrete' or 'continuous' formulation. One of the conclusions in Högberg & Berggren (2000) was that a continuous formulation is a good enough approximation if control is performed on a problem with a dominating instability. Here, the analysis is done for dominating instabilities using the PSE so a continuous approach has been chosen for the derivation of the adjoint equations.

B.1. *Inner product*

For a compact notation of the adjoint equations, we will use the *formal adjoint* L^* for the differential operator L defined by the relation

$$(\psi, L\phi)=(L^*\psi,\phi)+\text{boundary terms}, \tag{B 1}$$

where the inner product $(\cdot,\cdot)$ is defined as

$$(\phi,\psi)=\int_{Z_0}^{Z_1}\int_{X_0}^{X_1}\int_0^{\infty}\phi^H\psi\,\mathrm{d}y\,\mathrm{d}x\,\mathrm{d}z, \tag{B 2}$$

for $\mathbb{C}^n$-valued functions ϕ and ψ. Here, the superscript * denotes adjoint quantities and ψ is denoted the *co-state variable* which is chosen such that it satisfies the adjoint equations $L^*\psi=0$.

B.2. *Derivation of the gradient*

The idea behind the derivation is to identify the gradient from the boundary terms in (B 1). There are earlier results on the derivation of the APSE (see Airiau 2000; Hill

https://doi.org/10.1017/S0022112002001301 Published online by Cambridge University Press

1997*a*); however in this analysis, as in Pralits *et al.* (2000*a*), the approach is somewhat different.

Here, we use a perturbation technique together with integration by parts in space. The APSE are derived directly from the PSE so the auxiliary condition also has to be taken into account. Further, there is no ansatz made on the co-state variables of the PSE such as (2.5). In this way a method has been introduced to derive the APSE which provides the corresponding adjoint auxiliary condition. The details of the derivation are given below. First, the objective function and the state equations are differentiated with respect to the control V_w. Differentiating (2.9) and (2.6)–(2.7) yields

$$\delta J = \mathrm{Re}\left\{\int_{Z_0}^{Z_1}\int_{X_0}^{X_1}\int_0^\infty \delta \boldsymbol{u}^H \boldsymbol{u}\,\mathrm{d}y\,\mathrm{d}x\,\mathrm{d}z + l^2\int_{Z_0}^{Z_1}\int_{X_0}^{X_1}\delta V_w V_w\,\mathrm{d}x\,\mathrm{d}z\right\}, \tag{B 3}$$

$$\boldsymbol{A}\delta\hat{q} + \boldsymbol{B}\frac{\partial\delta\hat{q}}{\partial y} + \boldsymbol{C}\frac{\partial^2\delta\hat{q}}{\partial y^2} + \boldsymbol{D}\frac{\partial\delta\hat{q}}{\partial x} + \left(\frac{\partial\boldsymbol{A}}{\partial Q}\delta Q + \frac{\partial\boldsymbol{A}}{\partial\alpha}\delta\alpha + \frac{\partial\boldsymbol{B}}{\partial Q}\delta Q + \frac{\partial\boldsymbol{D}}{\partial Q}\delta Q\right)\hat{q} = 0, \tag{B 4}$$

$$\int_0^\infty \left(\delta\hat{\boldsymbol{u}}^H\frac{\partial\hat{\boldsymbol{u}}}{\partial x} + \hat{\boldsymbol{u}}^H\frac{\partial\delta\hat{\boldsymbol{u}}}{\partial x}\right)\mathrm{d}y = 0. \tag{B 5}$$

The variations δq, δQ are the variations of q, Q caused by the variation of V_w. Note also that the variation of q results in a variation of both the amplitude function $\hat{q}$ and the streamwise wavenumber α:

$$\delta q = \delta\hat{q}\Theta + \hat{q}\Theta\int_{X_0}^{x'}\delta\alpha\,\mathrm{d}x', \tag{B 6}$$

where

$$\Theta = \exp\mathrm{i}\left(\int_{X_0}^{x'}\alpha\,\mathrm{d}x' + \beta z - \omega t\right).$$

Proceed by differentiating (2.1)–(2.3). This is given in a compact form as

$$\frac{\partial L_{BLE}}{\partial Q}\delta Q Q + L_{BLE}\delta Q = 0. \tag{B 7}$$

Now, introduce the complex functions $q^* = (p^*, u^*, v^*, w^*)^T$ and r^*, the so-called co-state variables, which are multiplied by (B 4)–(B 5) respectively according to (B 2). Then (B 7) are multiplied by the co-state variables $Q^* = (V^*, U^*, W^*)^T$ in the same manner. The corresponding left-hand side of (B 1) can now be written

$$\begin{aligned}
&\int_{Z_0}^{Z_1}\int_{X_0}^{X_1}\int_0^\infty q^{*H}\left(\boldsymbol{A}\delta\hat{q} + \boldsymbol{B}\frac{\partial\delta\hat{q}}{\partial y} + \boldsymbol{C}\frac{\partial^2\delta\hat{q}}{\partial y^2} + \boldsymbol{D}\frac{\partial\delta\hat{q}}{\partial x} + \frac{\partial\boldsymbol{A}}{\partial Q}\delta Q\hat{q} + \frac{\partial\boldsymbol{A}}{\partial\alpha}\delta\alpha\hat{q}\right.\\
&\qquad\left.+\frac{\partial\boldsymbol{B}}{\partial Q}\delta Q\hat{q} + \frac{\partial\boldsymbol{D}}{\partial Q}\delta Q\hat{q}\right)\mathrm{d}y\,\mathrm{d}x\,\mathrm{d}z + \mathrm{c.c.}\\
&\qquad+\int_{Z_0}^{Z_1}\int_{X_0}^{X_1}\int_0^\infty\left(\overline{r^*}\left(\delta\hat{\boldsymbol{u}}^H\frac{\partial\hat{\boldsymbol{u}}}{\partial x} + \hat{\boldsymbol{u}}^H\frac{\partial\delta\hat{\boldsymbol{u}}}{\partial x}\right) + r^*\left(\delta\hat{\boldsymbol{u}}^T\frac{\partial\bar{\hat{\boldsymbol{u}}}}{\partial x} + \hat{\boldsymbol{u}}^T\frac{\partial\delta\bar{\hat{\boldsymbol{u}}}}{\partial x}\right)\right)\mathrm{d}y\,\mathrm{d}x\,\mathrm{d}z\\
&\qquad+\int_{Z_0}^{Z_1}\int_{X_0}^{X_1}\int_0^\infty Q^{*T}\left(\frac{\partial L_{BLE}}{\partial Q}\delta Q Q + L_{BLE}\delta Q\right)\mathrm{d}y\,\mathrm{d}x\,\mathrm{d}z.
\end{aligned} \tag{B 8}$$

https://doi.org/10.1017/S0022112002001301 Published online by Cambridge University Press

The right-hand side of (B 1) is derived by removing the derivatives from the differentiated state equations using integration by parts in Ω. Note here that the co-state variable r^* has been introduced due to the additional equation, (2.7), of the PSE. Further, the complex conjugate has been added as the gradient by definition, (2.11), is a real-valued function.

Here, the complex conjugate is written out explicitly for the auxiliary condition. Note that $\delta\alpha$ terms in (B 8) now must be integrated in the x-direction in order to obtain the same integral form as in (B 6).

After collecting terms of $\delta\hat{\boldsymbol{u}}$, $\delta\hat{q}$, δQ and $\int_{X_0}^{x'}\delta\alpha\,\mathrm{d}x'$, the right-hand side including boundary terms is written

$$
\begin{aligned}
&\int_{Z_0}^{Z_1}\int_{X_0}^{X_1}\int_0^{\infty}\left(\boldsymbol{A}^H q^* - \boldsymbol{B}^H\frac{\partial q^*}{\partial y} + \boldsymbol{C}^H\frac{\partial^2 q^*}{\partial y^2} - \boldsymbol{D}^H\frac{\partial q^*}{\partial x}\right)\delta\hat{q}\,\mathrm{d}y\,\mathrm{d}x\,\mathrm{d}z + \text{c.c.}\\
&+\int_{Z_0}^{Z_1}\int_{X_0}^{X_1}\int_0^{\infty}\left((r^* - \overline{r^*})\frac{\partial\bar{\hat{\boldsymbol{u}}}}{\partial x} + \frac{\partial r^*}{\partial x}\bar{\hat{\boldsymbol{u}}}\right)\delta\hat{\boldsymbol{u}}\,\mathrm{d}y\,\mathrm{d}x\,\mathrm{d}z + \text{c.c.}\\
&+\int_{Z_0}^{Z_1}\int_{X_0}^{X_1}\int_0^{\infty}(L^*_{BLE}(Q)Q^* - f_{ABLE})\delta Q\,\mathrm{d}y\,\mathrm{d}x\,\mathrm{d}z\\
&-\int_{Z_0}^{Z_1}\int_{X_0}^{X_1}\int_0^{\infty}\frac{\partial}{\partial x}\left(q^{*H}\frac{\partial\boldsymbol{A}}{\partial\alpha}\hat{q}\right)\int_{X_0}^{x'}\delta\alpha\,\mathrm{d}x'\,\mathrm{d}y\,\mathrm{d}x\,\mathrm{d}z\\
&+\int_{Z_0}^{Z_1}\int_{X_0}^{X_1}\int_0^{\infty}U_e\frac{\partial U^*}{\partial x}\delta U_e\,\mathrm{d}y\,\mathrm{d}x\,\mathrm{d}z\\
&+\int_{Z_0}^{Z_1}\int_0^{\infty}\Bigg(\Bigg[q^{*H}\boldsymbol{D}\delta\hat{q} + \overline{r^*}\hat{\boldsymbol{u}}^H\delta\hat{\boldsymbol{u}} + q^{*H}\frac{\partial\boldsymbol{A}}{\partial\alpha}\hat{q}\int_{X_0}^{x'}\delta\alpha\,\mathrm{d}x' + \bar{u}^*\hat{u}\delta U + \bar{w}^*\hat{u}\delta W\\
&+V^*\delta U + UU^*\delta U + U^*\delta P + W^*U\delta W - U^*U_e\delta U_e\Bigg]_{X_0}^{X_1}\Bigg)\mathrm{d}y\,\mathrm{d}z\\
&+\int_{Z_0}^{Z_1}\int_{X_0}^{X_1}\Bigg(\Bigg[q^{*H}\boldsymbol{B}\delta\hat{q} + q^{*H}\boldsymbol{C}\frac{\partial\delta\hat{q}}{\partial y} - \frac{\partial(q^{*H}\boldsymbol{C})}{\partial y}\delta\hat{q} + \bar{u}^*\hat{v}\delta U\\
&+\bar{v}^*\hat{v}\delta V + \bar{w}^*\hat{v}\delta W + V^*\delta V + VU^*\delta U + W^*V\delta W\\
&+\frac{1}{Re}(U_y^*\delta U + W_y^*\delta W - W^*\delta W_y - U^*\delta U_y)\Bigg]_0^{\infty}\Bigg)\mathrm{d}x\,\mathrm{d}z. \qquad \text{(B 9)}
\end{aligned}
$$

Here, f_{ABLE} are the terms due to δQ in the PSE. In order to identify the objective function (B 3) in (B 9), we add and subtract the energy norm in (B 9). Using (B 6), this additional term can be written

$$
\int_{Z_0}^{Z_1}\int_{X_0}^{X_1}\int_0^{\infty}\left(\delta\boldsymbol{u}^H\boldsymbol{u} - \delta\hat{\boldsymbol{u}}^H\hat{\boldsymbol{u}}|\Theta|^2 - \mathrm{i}|\hat{\boldsymbol{u}}|^2\int_{X_0}^{x'}\delta\alpha\,\mathrm{d}x'|\Theta|^2\right)\mathrm{d}y\,\mathrm{d}x\,\mathrm{d}z + \text{c.c.} \qquad \text{(B 10)}
$$

https://doi.org/10.1017/S0022112002001301 Published online by Cambridge University Press

Now impose the following boundary conditions on the state and co-state variables:

$$\begin{aligned}
&\delta\hat{u} = \delta\hat{v} = \delta\hat{w} = 0 && \text{at} \quad y = 0,\\
&\delta\hat{u}, \delta\hat{v}, \delta\hat{w}, \delta\hat{p} \to 0 && \text{as} \quad y \to \infty,\\
&\delta\hat{u} = \delta\hat{v} = \delta\hat{w} = \delta\hat{p} = 0 && \text{at} \quad x = X_0,\\
&\delta\ U = \delta\ W = 0 && \text{at} \quad y = 0,\\
&\delta\ U, \delta\ W \to 0 && \text{as} \quad y \to \infty,\\
&\delta U = \delta W = \delta U_e = 0 && \text{at} \quad x = X_0,\\
&u^* = v^* = w^* = 0 && \text{at} \quad y = 0,\\
&u^*, v^*, w^*, p^* \to 0 && \text{as} \quad y \to \infty,\\
&U^* = W^* = 0 && \text{at} \quad y = 0,\\
&U^*, V^*, W^* \to 0 && \text{as} \quad y \to \infty.
\end{aligned}$$

Let q^* and r^* satisfy the equations given by $\delta\boldsymbol{u}$, $\delta\hat{q}$ and $\int_{X_0}^{x'}\delta\alpha\,\mathrm{d}x'$. Further, let Q^* satisfy the equations given by δQ. This is written explicitly as

$$\begin{aligned}
&\bar{p}^*\mathrm{i}\alpha - \frac{\partial\bar{p}^*}{\partial x} + \frac{\partial\bar{u}^*}{\partial y}V - \frac{\partial\bar{u}^*}{\partial x}U + \bar{w}^*\frac{\partial W}{\partial x} - \frac{1}{Re}\frac{\partial^2\bar{u}^*}{\partial y^2}\\
&\qquad + \bar{u}^*\left[-\mathrm{i}\omega + \mathrm{i}\alpha U + \frac{\partial U}{\partial x} + \mathrm{i}\beta W + \frac{1}{Re}(\alpha^2+\beta^2)\right]\\
&\qquad = -(r^* - \overline{r^*})\frac{\partial\bar{\hat{u}}}{\partial x} + \frac{\partial\overline{r^*}}{\partial x}\bar{\hat{u}} + \bar{\hat{u}}|\Theta|^2, \qquad \text{(B 11)}
\end{aligned}$$

$$\begin{aligned}
&\frac{\partial\bar{p}^*}{\partial y} + \bar{u}^*\frac{\partial U}{\partial y} - \frac{\partial\bar{v}^*}{\partial y}V - \frac{\partial\bar{v}^*}{\partial x}U + \bar{w}^*\frac{\partial W}{\partial y} - \frac{1}{Re}\frac{\partial^2\bar{v}^*}{\partial y^2}\\
&\qquad + \bar{v}^*\left[-\mathrm{i}\omega + \mathrm{i}\alpha U + \frac{\partial V}{\partial y} + \mathrm{i}\beta W + \frac{1}{Re}(\alpha^2+\beta^2)\right]\\
&\qquad = -(r^* - \overline{r^*})\frac{\partial\bar{\hat{v}}}{\partial x} + \frac{\partial\overline{r^*}}{\partial x}\bar{\hat{v}} + \bar{\hat{v}}|\Theta|^2, \qquad \text{(B 12)}
\end{aligned}$$

$$\begin{aligned}
&\bar{p}^*\mathrm{i}\beta - \frac{\partial\bar{w}^*}{\partial y}V - \frac{\partial\bar{w}^*}{\partial x}U - \frac{1}{Re}\frac{\partial^2\bar{w}^*}{\partial y^2} + \bar{w}^*\left[-\mathrm{i}\omega + \mathrm{i}\alpha U + \mathrm{i}\beta W + \frac{1}{Re}(\alpha^2+\beta^2)\right]\\
&\qquad = -(r^* - \overline{r^*})\frac{\partial\bar{\hat{w}}}{\partial x} + \frac{\partial\overline{r^*}}{\partial x}\bar{\hat{w}} + \bar{\hat{w}}|\Theta|^2, \qquad \text{(B 13)}
\end{aligned}$$

$$-\frac{\partial\bar{u}^*}{\partial x} + \bar{u}^*\mathrm{i}\alpha - \frac{\partial\bar{v}^*}{\partial y} + \bar{w}^*\mathrm{i}\beta = 0, \qquad \text{(B 14)}$$

$$\frac{\partial}{\partial x}\int_0^\infty \left(\mathrm{i}(\bar{p}^*\hat{u} + \bar{u}^*\hat{p}) + \left(\mathrm{i}U + \frac{2\alpha}{Re}\right)(\bar{u}^*\hat{u} + \bar{v}^*\hat{v} + \bar{w}^*\hat{w})\right)\mathrm{d}y + \mathrm{i}|\Theta|^2\int_0^\infty |\hat{\boldsymbol{u}}|^2\,\mathrm{d}y = 0, \qquad \text{(B 15)}$$

$$\frac{\partial V^*}{\partial y} - \frac{\partial U}{\partial y}U^* - W^*\frac{\partial W}{\partial y} = \mathrm{Re}\left\{\bar{u}^*\frac{\partial\hat{u}}{\partial y} - \frac{\partial\bar{v}^*}{\partial y}\hat{v} + \bar{w}^*\frac{\partial\hat{w}}{\partial y}\right\}, \qquad \text{(B 16)}$$

https://doi.org/10.1017/S0022112002001301 Published online by Cambridge University Press

$$\frac{\partial V^*}{\partial x} + U\frac{\partial U^*}{\partial x} + \frac{\partial V}{\partial y}U^* + V\frac{\partial U^*}{\partial y} - W^*\frac{\partial W}{\partial x} + \frac{1}{Re}\frac{\partial^2 U^*}{\partial y^2}$$
$$= \mathrm{Re}\left\{\mathrm{i}\alpha[\bar{u}^*\hat{u} + \bar{v}^*\hat{v} + \bar{w}^*\hat{w}] - \frac{\partial \bar{u}^*}{\partial x}\hat{u} - \frac{\partial \bar{u}^*}{\partial y}\hat{v} - \bar{u}^*\frac{\partial \hat{v}}{\partial y} + \bar{v}^*\frac{\partial \hat{v}}{\partial x} + \bar{w}^*\frac{\partial \hat{w}}{\partial x}\right\}, \quad \text{(B 17)}$$

$$\frac{\partial W^*}{\partial x}U + \frac{\partial W^*}{\partial y}V + \frac{1}{Re}\frac{\partial^2 W^*}{\partial y^2}$$
$$= \mathrm{Re}\left\{\mathrm{i}\beta[\bar{u}^*\hat{u} + \bar{v}^*\hat{v} + \bar{w}^*\hat{w}] - \frac{\partial \bar{w}^*}{\partial x}\hat{u} - \bar{w}^*\frac{\partial \hat{u}}{\partial x} - \frac{\partial \bar{w}^*}{\partial y}\hat{v} - \bar{w}^*\frac{\partial \hat{v}}{\partial y}\right\}. \quad \text{(B 18)}$$

Equations (B 11)–(B 15) are the adjoint of the parabolized stability equation, APSE. The inhomogenous right-hand side of (B 11)–(B 13), here denoted f_{APSE}, comes from the auxiliary condition (2.7) and the objective function (2.9). Equation (B 15) solves the additional unknown co-state variable r^* iteratively at each streamwise position. Equations (B 16)–(B 18) are the adjoint of the boundary layer equations, ABLE. The inhomogeneous right-hand side, denoted f_{ABLE}, is calculated from the solution of the PSE and the APSE. However, only the real part is used as the left-hand side consists of real-valued equations. The remaining boundary terms in (B 9) come from the boundary $x = X_1$ and the δV term at $y = 0$. We impose the initial condition of both the ABLE and APSE to be zero at $x = X_1$. This does not cause trivial solutions as both (B 11)–(B 15) and (B 16)–(B 18) have a non-zero right-hand side in Ω. The remaining terms from (B 9) can now be written

$$\mathrm{Re}\left\{\delta J - \int_{Z_0}^{Z_1}\int_{X_0}^{X_1}((l^2 V_\mathrm{w} + V_\mathrm{w}^*)\delta V_\mathrm{w})\,\mathrm{d}x\,\mathrm{d}z + \int_{Z_0}^{Z_1}\int_{X_0}^{X_1}\int_0^\infty U_e\frac{\partial U^*}{\partial x}\delta U_e\,\mathrm{d}y\,\mathrm{d}x\,\mathrm{d}z\right\} = 0. \quad \text{(B 19)}$$

Index w here denotes the value at $y = 0$. Equation (B 19) can now be rewritten as

$$\delta J = \int_{Z_0}^{Z_1}\int_{X_0}^{X_1}((l^2 V_\mathrm{w} + V_\mathrm{w}^*)\delta V_\mathrm{w})\,\mathrm{d}x\,\mathrm{d}z - \int_{Z_0}^{Z_1}\int_{X_0}^{X_1}\int_0^\infty U_e\frac{\partial U^*}{\partial x}\delta U_e\,\mathrm{d}y\,\mathrm{d}x\,\mathrm{d}z. \quad \text{(B 20)}$$

If the first term on the right-hand side of (B 20) is written, using (2.11), as

$$\delta J = \int_{Z_0}^{Z_1}\int_{X_0}^{X_1}\nabla_{V_\mathrm{w}} J\,\delta V_\mathrm{w}\,\mathrm{d}x\,\mathrm{d}z, \quad \text{(B 21)}$$

then the gradient of the objective function with respect to the wall-normal velocity component of the mean flow at the wall can be identified as

$$\nabla_{V_\mathrm{w}} J = l^2 V_\mathrm{w} + V_\mathrm{w}^* \quad \text{on} \quad y = 0. \quad \text{(B 22)}$$

The second term on the right-hand side of (B 20) is the variation of the objective function due a variation of the free-stream velocity. If a similar gradient definition as in (B 21) is used for U_e

$$\delta J = \int_{Z_0}^{Z_1}\int_{X_0}^{X_1}\int_0^\infty \nabla_{U_e} J\,\delta U_e\,\mathrm{d}y\,\mathrm{d}x\,\mathrm{d}z, \quad \text{(B 23)}$$

then the gradient of the objective function with respect to the free-stream velocity can be written

$$\nabla_{U_e} J = -U_e\int_0^\infty \frac{\partial U^*}{\partial x}\,\mathrm{d}y. \quad \text{(B 24)}$$

https://doi.org/10.1017/S0022112002001301 Published online by Cambridge University Press

The variation U_e would be the consequence of, for example, a change in the geometry and consequently the free-stream pressure, and is therefore not considered in this paper.

B.3. *Derivation of the gradient including stabilization*

The derivation of the gradient including the stabilization terms does not differ much from the derivation in § B.2. The same definition of the adjoint, (B 1), and inner product, (B 2), are used. The difference becomes clear if the stabilization terms are added to (B 8). This can be written

$$\begin{aligned}
&\int_{Z_0}^{Z_1}\int_{X_0}^{X_1}\int_0^{\infty} q^{*H}\left(\boldsymbol{A}\delta\hat{q}+\boldsymbol{B}\frac{\partial\delta\hat{q}}{\partial y}+\boldsymbol{C}\frac{\partial^2\delta\hat{q}}{\partial y^2}+\boldsymbol{D}\frac{\partial\delta\hat{q}}{\partial x}+\frac{\partial\boldsymbol{A}}{\partial Q}\delta Q\hat{q}+\frac{\partial\boldsymbol{A}}{\partial\alpha}\delta\alpha\hat{q}\right.\\
&\qquad\left.+\frac{\partial B}{\partial Q}\delta Q\hat{q}+\frac{\partial D}{\partial Q}\delta Q\hat{q}\right)\mathrm{d}y\,\mathrm{d}x\,\mathrm{d}z+\text{c.c.}\\
&\qquad+s\int_{Z_0}^{Z_1}\int_{X_0}^{X_1}\int_0^{\infty} q^{*H}\left(\boldsymbol{A}\frac{\partial\delta\hat{q}}{\partial x}+\boldsymbol{B}\frac{\partial}{\partial x}\left(\frac{\partial\delta\hat{q}}{\partial y}\right)+\boldsymbol{C}\frac{\partial}{\partial x}\left(\frac{\partial^2\delta\hat{q}}{\partial y^2}\right)+\frac{\partial\boldsymbol{A}}{\partial Q}\delta Q\frac{\partial\delta\hat{q}}{\partial x}\right.\\
&\qquad\left.+\frac{\partial\boldsymbol{A}}{\partial\alpha}\delta\alpha\frac{\partial\delta\hat{q}}{\partial x}+\frac{\partial\boldsymbol{B}}{\partial Q}\delta Q\frac{\partial\delta\hat{q}}{\partial x}\right)\mathrm{d}y\,\mathrm{d}x\,\mathrm{d}z+\text{c.c.}\\
&\qquad+\int_{Z_0}^{Z_1}\int_{X_0}^{X_1}\int_0^{\infty}\left(\overline{r^*}\left(\delta\hat{\boldsymbol{u}}^H\frac{\partial\hat{\boldsymbol{u}}}{\partial x}+\hat{\boldsymbol{u}}^H\frac{\partial\delta\hat{\boldsymbol{u}}}{\partial x}\right)+r^*\left(\delta\hat{\boldsymbol{u}}^T\frac{\partial\bar{\hat{\boldsymbol{u}}}}{\partial x}+\hat{\boldsymbol{u}}^T\frac{\partial\delta\bar{\hat{\boldsymbol{u}}}}{\partial x}\right)\right)\mathrm{d}y\,\mathrm{d}x\,\mathrm{d}z\\
&\qquad+\int_{Z_0}^{Z_1}\int_{X_0}^{X_1}\int_0^{\infty} Q^{*T}\left(\frac{\partial L_{BLE}}{\partial Q}\delta QQ+L_{BLE}\delta Q\right)\mathrm{d}y\,\mathrm{d}x\,\mathrm{d}z. \qquad \text{(B 25)}
\end{aligned}$$

The new terms only appear in the second integral expression in (B 25). However, this expression includes $\delta\hat{q}$, $\delta\alpha$ and δQ so (B 11)–(B 15) and (B 16)–(B 18) will all have additional terms due to s. The full derivation of the gradient using (B 25) is not necessary due to the resemblance between (B 8) and (B 25). Instead, it suffices to evaluate the additional terms associated with the stabilization. This is done following the steps in § B.2 and yields

$$\begin{aligned}
&s\left(\frac{\partial\bar{p}^*}{\partial x}\mathrm{i}\alpha-\frac{\partial^2\bar{u}^*}{\partial x\partial y}V+\frac{\partial\bar{w}^*}{\partial x}\frac{\partial W}{\partial x}-\frac{\partial\bar{u}^*}{\partial x}\frac{\partial V}{\partial y}-\frac{1}{Re}\frac{\partial^3\bar{u}^*}{\partial x\partial y^2}\right.\\
&\qquad\left.+\frac{\partial\bar{u}^*}{\partial x}\left[-\mathrm{i}\omega+\mathrm{i}\alpha U+\frac{\partial U}{\partial x}+\mathrm{i}\beta W+\frac{1}{Re}(\alpha^2+\beta^2)\right]\right), \qquad \text{(B 26)}\\
&s\left(-\frac{\partial^2\bar{p}^*}{\partial x\partial y}+\frac{\partial\bar{u}^*}{\partial x}\frac{\partial U}{\partial y}-\frac{\partial^2\bar{v}^*}{\partial x\partial y}V-\frac{\partial\bar{v}^*}{\partial x}\frac{\partial V}{\partial y}+\frac{\partial\bar{w}^*}{\partial x}\frac{\partial W}{\partial y}-\frac{1}{Re}\frac{\partial^3\bar{v}^*}{\partial x\partial y^2}\right.\\
&\qquad\left.+\frac{\partial\bar{v}^*}{\partial x}\left[-\mathrm{i}\omega+\mathrm{i}\alpha U+\frac{\partial V}{\partial y}+\mathrm{i}\beta W+\frac{1}{Re}(\alpha^2+\beta^2)\right]\right), \qquad \text{(B 27)}\\
&s\left(\frac{\partial\bar{p}^*}{\partial x}\mathrm{i}\beta-\frac{\partial^2\bar{w}^*}{\partial x\partial y}V-\frac{\partial\bar{w}^*}{\partial x}\frac{\partial V}{\partial y}-\frac{1}{Re}\frac{\partial^3\bar{w}^*}{\partial x\partial y^2}\right.\\
&\qquad\left.+\frac{\partial\bar{w}^*}{\partial x}\left[-\mathrm{i}\omega+\mathrm{i}\alpha U+\mathrm{i}\beta W+\frac{1}{Re}(\alpha^2+\beta^2)\right]\right), \qquad \text{(B 28)}
\end{aligned}$$

https://doi.org/10.1017/S0022112002001301 Published online by Cambridge University Press

$$s\left(\frac{\partial \bar{u}^*}{\partial x}\mathrm{i}\alpha - \frac{\partial^2 \bar{v}^*}{\partial x \partial y} + \frac{\partial \bar{w}^*}{\partial x}\mathrm{i}\beta\right), \tag{B 29}$$

$$s\int_0^\infty \left(\frac{\partial}{\partial x}\left[\mathrm{i}\left(\bar{p}^*\frac{\partial \hat{u}}{\partial x} + \bar{u}^*\frac{\partial \hat{p}}{\partial x}\right) + \left(\mathrm{i}U + \frac{2\alpha}{Re}\right)\left(\bar{u}^*\frac{\partial \hat{u}}{\partial x} + \bar{v}^*\frac{\partial \hat{v}}{\partial x} + \bar{w}^*\frac{\partial \hat{w}}{\partial x}\right)\right]\right)\mathrm{d}y, \tag{B 30}$$

$$s\left(\mathrm{Re}\left\{\bar{u}^*\frac{\partial^2 \hat{u}}{\partial x \partial y} - \frac{\partial \bar{v}^*}{\partial y}\frac{\partial \hat{v}}{\partial x} + \bar{w}^*\frac{\partial^2 \hat{w}}{\partial x \partial y}\right\}\right), \tag{B 31}$$

$$s\left(\mathrm{Re}\left\{\mathrm{i}\alpha\left[\bar{u}^*\frac{\partial \hat{u}}{\partial x} + \bar{v}^*\frac{\partial \hat{v}}{\partial x} + \bar{w}^*\frac{\partial \hat{w}}{\partial x}\right] - \frac{\partial}{\partial x}\left(\bar{u}^*\frac{\partial \hat{u}}{\partial x}\right) - \frac{\partial}{\partial y}\left(\bar{u}^*\frac{\partial \hat{v}}{\partial x}\right)\right\}\right), \tag{B 32}$$

$$s\left(\mathrm{Re}\left\{\mathrm{i}\beta\left[\bar{u}^*\frac{\partial \hat{u}}{\partial x} + \bar{v}^*\frac{\partial \hat{v}}{\partial x} + \bar{w}^*\frac{\partial \hat{w}}{\partial x}\right] - \frac{\partial}{\partial x}\left(\bar{w}^*\frac{\partial \hat{u}}{\partial x}\right) - \frac{\partial}{\partial y}\left(\bar{w}^*\frac{\partial \hat{v}}{\partial x}\right)\right\}\right). \tag{B 33}$$

Equations (B 26)–(B 29) are the additional terms in (B 11)–(B 14) respectively. Equation (B 30) is the additional term in (B 15) and (B 31)–(B 33) are the additional terms in (B 16)–(B 18) respectively. It should be noted here that the boundary conditions do not change in any of the state or adjoint equations. Further, the gradient expression does not have any additional terms due to the stabilization parameter s.

REFERENCES

Airiau, C. 2000 Non-parallel acoustic receptivity of a Blasius boundary layer using an adjoint approach. *Flow, Turbulence Combust.* **65**, 347–367.

Andersson, P., Berggren, M. & Henningson, D. 1999 Optimal disturbances and bypass transition in boundary layers. *Phys. Fluids* **11**, 134–150.

Andersson, P., Henningson, D. S. & Hanifi, A. 1998 On a stabilization procedure for the parabolic stability equations. *J. Engng Maths* **33**, 311–332.

Balakumar, P. & Hall, P. 1999 Optimum suction distribution for transition prediction. *Theor. Comput. Fluid Dyn.* **13**, 1–19.

Bertolotti, F., Herbert, T. & Spalart, S. 1992 Linear and nonlinear stability of the Blasius boundary layer. *J. Fluid Mech.* **242**, 441–474.

Bewley, T. & Liu, S. 1998 Optimal and robust control and estimation of linear paths to transition. *J. Fluid Mech.* **365**, 305–349.

Bewley, T. & Moin, P. 1997 Optimal and robust approaches for linear and nonlinear regulation problems in fluid mechanics. *AIAA Paper* 97-1872.

Byrd, R., Lu, P., Nocedal, J. & Zhu, C. 1995 A limited memory algorithm for bound constrained optimization. *SIAM J. Sci. Comput.* **16**, 1190–1208.

Dobrinsky, A. & Collis, S. S. 2000 Adjoint parabolized stability equations for receptivity prediction. *AIAA Paper* 2000-2651.

Haj-Hariri, H. 1994 Characteristics analysis of the parabolized stability equations. *Stud. Appl. Maths* **92**, 41–53.

Herbert, T. 1997 Parabolized stability equations. *Annu. Rev. Fluid Mech.* **29**, 245–283.

Hill, D. C. 1997*a* Receptivity in non-parallel boundary layers. In *ASME Fluids Engineering Division Summer Meeting, FEDSM '97*.

Hill, D. C. 1997*b* Inverse design for laminar three-dimensional boundary layers. *Bull. Am. Phys. Soc.* **42**, 2120.

Högberg, M. & Berggren, M. 2000 Numerical approaches to optimal control of a model equation for shear flow instabilities. *Flow, Turbulence Combust.* **65**, 299–320.

Högberg, M. & Henningson, D. S. 1998 Secondary instability of cross-flow vortices in Falkner-Skan-Cooke boundary layers. *J. Fluid Mech.* **368**, 339–357.

Iglisch, R. 1949 Exakte berechnung der laminaren reibungsschicht an der längsangeströmten ebenen platte mit homogener absaugung. *NACA RM* 1205.

https://doi.org/10.1017/S0022112002001301 Published online by Cambridge University Press

Joslin, R. 1998 Overview of laminar flow control. *Tech. Rep.* 1998-208705. NASA, Langley Research Center, Hampton, Virginia.

Li, F. & Malik, M. R. 1994 Mathematical nature of parabolized stability equations. In *4th IUTAM Symp. on Laminar-Turbulent Transition, Sendi, Japan* (ed. R. Kobayashi), pp. 205–212. Springer.

Li, F. & Malik, M. R. 1996 On the nature of pse approximation. *Theor. Comput. Fluid Dyn.* **8**, 253–273.

Malik, M. R. & Balakumar, P. 1992 Nonparallel stability of rotating disk flow using pse. In *Instability, Transition and Turbulence* (ed. M. Hussaini, A. Kumar & C. Streett), pp. 168–180. Springer.

Pralits, J. O., Airiau, C., Hanifi, A. & Henningson, D. S. 2000*a* Sensitivity analysis using adjoint parabolized stability equations for compressible flows. *Flow, Turbulence Combust.* **65**, 321–346.

Pralits, J. O., Hanifi, A. & Henningson, D. S. 2000*b* Adjoint-based suction optimization for 3d boundary layer flows. *Tech. Rep.* FFA TN 2000-58. Swedish Defence Research Agency, FOI, Aeronautics Division, FFA, SE-172 90 Stockholm, Sweden.

Schlichting, H. 1979 *Boundary-Layer Theory*, 7th edn. McGraw-Hill.

Simen, M. 1992 Local and non-local stability theory of spatially varying flows. In *Instability, Transition and Turbulence* (ed. M. Hussaini, A. Kumar & C. Streett), pp. 181–201. Springer.

Ulrich, A. 1944 Theoretishce untersuchungen über die widerstandsersparnis durch laminarhaltung mit absaugung. *Schriften dt. Adad. d. Luftfahrtforschung* **8 B**, No. 2.

Walther, S., Airiau, C. & Bottaro, A. 2001 Optimal control of Tollmien–Schlichting waves in a developing boundary layer. *Phys. Fluids* **13**, 2087–2096.

Zhu, C., Byrd, R., Lu, P. & Nocedal, J. 1994 L-bfgs-b: Fortran subroutines for large scale bound constrained optimization. *Tech. Rep.* NAM-11. EECS Department, Northwestern University.

https://doi.org/10.1017/S0022112002001301 Published online by Cambridge University Press